



**NTNU – Trondheim**  
Norwegian University of  
Science and Technology

# Physical Modelling of Surge Tank Throttling

**Robert Stigen Landskaug**

Civil and Environmental Engineering (2 year)

Submission date: July 2015

Supervisor: Leif Lia, IVM

Co-supervisor: Kaspar Vereide, IVM

Norwegian University of Science and Technology  
Department of Hydraulic and Environmental Engineering



# M.Sc. THESIS IN HYDRAULIC ENGINEERING

Candidate: Mr. Robert Stigen Landskaug

Title: Physical Modelling of Surge Tank Throttling

## 1. Background

Surge tanks are applied in hydropower plants for dampening of water hammer, and to ensure regulation stability of the power plant. The surge tank may be constructed with a throttle, which introduce a singular loss when water is flowing into or out from the surge tank. Especially for hydropower pumped storage plants (PSP) the implementation of a throttle is beneficial due to the massive hydraulic transients occurring in such systems.

Due to the massive construction of wind and solar power in Europe, the need for large energy storage facilities is increasing. PSPs are effective at storing large amount of energy, and many new PSP projects are currently under development. This high development rate of new PSPs trigger the need for research in order to further develop this technology.

Modern PSPs are able to shift rapidly between pumping mode and turbine mode, which result in large hydraulic transients. In PSPs with surge tanks, a throttle is often applied in order to reduce the mass oscillations. Design of such throttles is a complex process, and the throttles are designed individually for each power plant. In order to gain further understanding of the throttle effect, and to improve the design of such structures, research is required.

## 2. Main questions for the thesis

The thesis shall cover, though not necessarily be limited to the main questions listed below.

### 2.1 Literature and desk study

The candidate shall carry out a literature study of relevant literature and theory.

### 2.2 Main tasks

The candidate must find and collect available background information such as former studies, reports and drawings. Related to this material the following must be carried out:

- 1 Literature review
  - a. Throttle effects
  - b. State-of-the-art throttle design
- 2 Description of the physical model facilities
- 3 Propose design for surge tank throttle
- 4 A priori estimation of throttle effect
- 5 Numerical simulation of throttle effect
- 6 Physical model testing of throttle effect
- 7 Conclusions
- 8 Proposals for future work
- 9 Presentation

### 3 Supervision and data input

Professor Leif Lia and PhD candidate Kaspar Vereide will supervise and assist the candidate, and make relevant information available.

Discussion with and input from colleagues and other research or engineering staff at NTNU, SINTEF and the hydropower industry is recommended. Significant inputs from other shall be referenced.

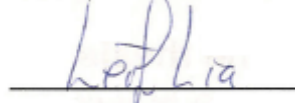
### 4 Report format, references and contract

The master contract must be signed not later than 15. January. The report should be written with a text editing software, and figures, tables, photos etc. should be of good quality. The report should contain an executive summary, a table of content, a list of figures and tables, a list of references and information about other relevant sources. The report should be submitted electronically in B5-format .pdf-file in DAIM, and three paper copies should be handed in to the institute.

The executive summary should not exceed 450 words, and should be suitable for electronic reporting.

The Master's thesis should be submitted within Wednesday 10<sup>th</sup> of June 2015.

Trondheim 14. January 2015



Leif Lia  
Professor

Department of Hydraulic and Environmental Engineering  
NTNU

# Abstract

The scope of this master thesis is to design a surge tank throttle based on literature values, and compare the expected head loss factor with the results from a 3D numerical simulation, and a physical model test. A literature review on throttle effects and the state-of-the-art throttle design will also be carried out as a part of the thesis. As a supplement to the thesis scope, the hydraulic effects of installing the throttle in the physical model will be discussed.

The literature review reveal that a throttle has a high influence on the dampening of mass oscillations in a hydropower plant. In addition, a properly designed throttle lowers the volume demand of the surge tank, improves the governing stability for the machines, and reduce the maximum pressure in front of the turbine.

The 1D numerical program LVTrans is used to calculate the hydraulic transients in the whole system and the 3D numerical program STAR-CCM+ is used to calculate the throttle head loss. The physical model used in this work is a 1:65 scale model of Torpa hydropower plant constructed at the Norwegian University of Science and Technology (NTNU).

The load case for the experiments is a multiple closing and opening case to get resonance and bring the system to the maximum possible state of oscillations, which is a method used in Austria since the 1960s. The throttle design tested in this work is an asymmetric throttle with a relatively simple design, to reduce construction time and cost. The main parameter for the throttle design was found to be the smallest diameter. Two surge tank throttles with different diameters were made and used to compare the different methods.

The literature values underestimate the head loss coefficient in both directions compared to the physical model test. The literature values show acceptable correlation to the physical model test in the upward direction, which is the direction with the simplest hydraulic conditions. The conditions in the downward direction are more complicated, and this is also reflected in the results, where the difference is larger.

The 3D numerical simulations give results that are lower than the physical model test for downward flow, and higher for upward flow. The numerical simulations give the highest ratio between head loss in the upward and downward directions.

The findings also shows a significant impact on the pressure development and dampening of mass oscillations by inserting a surge tank throttle, as was found in the literature review. The two throttles tested in the physical model reduced the maximum pressure by 5.2% and 3.9% for the smallest and largest throttle diameter respectively. This was with the use of the scaled maximum discharge from the prototype.



# Sammendrag

Formålet med denne masteroppgaven er å designe en strupning i et svingekammer, og deretter sammenligne de forventede falltapsfaktorene med resultater fra tredimensjonale numeriske simuleringer og fysiske modellforsøk. En litteraturstudie på strupningseffekter og rådende forskning innen strupningsdesign er også en del av oppgaven. I tillegg diskuteres effekten som oppnås ved å installere en strupning i den fysiske modellen.

Litteraturstudien viser at strupninger har stor innvirkning på demping av massesvingninger i vannkraftanlegg. I tillegg vil en riktig designet strupning senke volumbehovet for svingekammeret, bedre reguleringsstabiliteten til maskineriet og redusere det maksimale trykket foran turbinen.

Det endimensjonale numeriske programmet LVTrans benyttes til å beregne hydrauliske transienter i hele systemet, og det tredimensjonale programmet STAR-CCM+ benyttes til å beregne falltaptet i strupningene. Den fysiske modellen som blir benyttet er en 1:65 modell av Torpa kraftverk. Modellen er bygd på Norges teknisk- naturvitenskaplige universitet (NTNU).

Forsøkene gjennomføres med gjentatt lukking og åpning av turbinen (resonansavslag) for å oppnå størst mulige massesvingninger, en metode benyttet i Østerrike siden 1960-tallet. Strupningen blir designet som en asymmetrisk strupning med et forholdsvis enkelt design, dette for å redusere byggetiden og kostnadene. Den viktigste parameteren ble funnet å være den minste diameteren. Det ble designet og laget to strupninger med ulike diametere for å sammenligne de ulike metodene.

For vannstrømning oppover ga litteraturverdiene akseptable verdier sammenlignet med de fysiske modellforsøkene, og det er denne retningen som har de enkleste hydrauliske forholdene. For vannstrømning nedover er forholdene mer kompliserte og forskjellene større. I begge tilfeller ga litteraturverdiene lavere falltapskoeffisienter enn de fysiske modellforsøkene.

De numeriske simuleringene ga lavere resultater enn den fysiske modellen for vannstrømning nedover, og høyere for vannstrømning oppover. De numeriske simuleringene ga dermed de høyeste forholdstallene mellom falltapskoeffisientene opp og ned.

Resultatene viser også en klar innvirkning på trykkutviklingen og dempingen av massesvingningene når en strupning blir satt inn i modellen. Dette bekrefter funnene fra litteraturstudien. De to strupningene som ble testet reduserte det maksimale trykket med 5.2% og 3.9%, henholdsvis for den minste og største diameteren. Dette med den skalerte maksimale vannføringen fra prototypen.





# Preface

This thesis is written as a final assignment on a master study at the Norwegian University of Science and Technology. The work is conducted at the faculty of Engineering Science and Technology at the department of Hydraulic and Environmental Engineering. The project work is awarded with 30 ETCS credits, and is carried out over 20 weeks.

First of all I would like to thank my supervisors professor Leif Lia and PhD candidate Kaspar Vereide. I would like to thank Kaspar for good discussions and help with the work, and I would like to thank Leif for the good and inspiring lectures in hydropower and hydraulic engineering.

At last I would also like to thank Geir Tesaker for making the throttles for the physical model experiments, and for the quick fix when it was needed.

Ski, 03. July 2015

A handwritten signature in blue ink that reads "Robert Stigen Landskaug". The signature is written in a cursive style and is positioned above a horizontal line.

Robert Stigen Landskaug



# Content

- Abstract ..... i
- Sammendrag ..... iii
- Preface ..... v
- Content ..... vii
- List of figures ..... ix
- List of tables ..... xi
- List of symbols ..... xiii
- 1 Introduction ..... 1
  - 1.1 Background ..... 1
  - 1.2 Surge tanks ..... 2
- 2 Literature review ..... 5
  - 2.1 Surge tank throttles ..... 5
  - 2.2 Throttle types ..... 5
  - 2.3 Throttle design process ..... 7
  - 2.4 Asymmetric throttle design ..... 8
- 3 Theory ..... 13
  - 3.1 Hydraulic transients ..... 13
  - 3.2 Basic differential equations ..... 18
  - 3.3 The method of characteristics ..... 20
  - 3.4 Head loss ..... 22
  - 3.5 Local loss coefficients ..... 23
  - 3.6 CFD modelling ..... 26
- 4 Method ..... 31
  - 4.1 Physical model ..... 31
  - 4.2 1D simulations of the system ..... 34
  - 4.3 Physical modelling of the surge tank throttle ..... 40
  - 4.4 3D simulations of the throttle effects ..... 48
- 5 Results ..... 55
  - 5.1 First throttle design ..... 55
  - 5.2 Second throttle design ..... 58

5.3	Additional findings .....	60
6	Discussion .....	65
6.1	Throttle effects.....	65
6.2	Error sources.....	67
6.3	Additional findings .....	71
7	Conclusion.....	77
7.1	Suggestions for further work .....	77
	References .....	79

# List of figures

<i>Figure 1-1: Hydropower surge tank design, modified after Vereide et al. (2015).</i> .....	3
<i>Figure 2-1: A symmetric throttle to left, an asymmetric throttle in the middle and a reverse flow throttle (Steyrer, 1999) to the right.</i> .....	6
<i>Figure 2-2: Different throttles and dampening effect (Steyrer, 1999)</i> .....	7
<i>Figure 2-3: Pressure in front of turbine</i> .....	9
<i>Figure 2-4: Asymmetric throttle parameters.</i> .....	9
<i>Figure 2-5: Variation in throttle design, based on Richter et al. (2012b).</i> .....	10
<i>Figure 3-1: Development of water hammer, based on Guttormsen (2006)</i> .....	15
<i>Figure 3-2: Mass oscillations in power plant with a surge shaft</i> .....	17
<i>Figure 3-3: Control volume for derivation of the equation of motion. (Wylie et al., 1993)</i> ...	18
<i>Figure 3-4: Control volume for derivation of the continuity equation. (Wylie et al., 1993)</i> ...	19
<i>Figure 3-5: xt-network for solving the problem in simple pipes (Wylie et al., 1993).</i> .....	21
<i>Figure 3-6: Schematic diagram of flow with a sudden contraction (Idelchik, 1986).</i> .....	24
<i>Figure 3-7: Schematic diagram of flow at a sudden expansion (Idelchik, 1986).</i> .....	25
<i>Figure 3-8: Time series of water velocity (Olsen, 2012).</i> .....	27
<i>Figure 3-9: Polyhedral (left), tetrahedral (middle) and trimmed (right) meshes.</i> .....	29
<i>Figure 3-10: Two dimensional discretization molecule.</i> .....	29
<i>Figure 4-1: Physical model layout.</i> .....	31
<i>Figure 4-2: The physical model water system.</i> .....	32
<i>Figure 4-3: 1D numerical model overview.</i> .....	35
<i>Figure 4-4: Pressure in the air cushion surge chamber.</i> .....	38
<i>Figure 4-5: Pressure in front of the turbine.</i> .....	38
<i>Figure 4-6: Velocity profiles in pipes when the flow turns around (Nielsen, 1990).</i> .....	39
<i>Figure 4-7: Throttle parameters</i> .....	40
<i>Figure 4-8: Simplified and actual throttle geometry</i> .....	41
<i>Figure 4-9: First throttle design as built.</i> .....	43
<i>Figure 4-10: Photography of the first throttle design.</i> .....	44
<i>Figure 4-11: Construction pieces of the throttle.</i> .....	44
<i>Figure 4-12: Detail photography of the smallest diameter.</i> .....	45
<i>Figure 4-13: First throttle mounted in the physical model.</i> .....	45
<i>Figure 4-14: Second throttle design as built.</i> .....	47
<i>Figure 4-15: Imported surface to left and remeshed surface to right.</i> .....	49
<i>Figure 4-16: Polyhedral volume mesh with prism layer with two layers.</i> .....	50
<i>Figure 4-17: Volumetric control boxes for upward and downward flow.</i> .....	51
<i>Figure 5-1: Stock chart of the loss coefficients with upward flow for the 25 mm throttle.</i> .....	55

<i>Figure 5-2: Stock chart of the loss coefficients with downward flow for the 25 mm throttle. .</i>	<i>56</i>
<i>Figure 5-3: Loss coefficients 25 mm throttle upward flow. ....</i>	<i>57</i>
<i>Figure 5-4: Loss coefficients 25 mm throttle downward flow. ....</i>	<i>57</i>
<i>Figure 5-5: Stock chart of the loss coefficients with upward flow for the 23 mm throttle. ....</i>	<i>58</i>
<i>Figure 5-6: Stock chart of the loss coefficients with downward flow for the 23 mm throttle. .</i>	<i>59</i>
<i>Figure 5-7: Loss coefficients 23 mm throttle upward flow. ....</i>	<i>60</i>
<i>Figure 5-8: Loss coefficients 23 throttle downward flow. ....</i>	<i>60</i>
<i>Figure 5-9: Air cushion surge chamber air pressure with the 25 mm throttle. ....</i>	<i>61</i>
<i>Figure 5-10: Turbine pressure with the 25 mm throttle. ....</i>	<i>61</i>
<i>Figure 5-11: Air cushion surge chamber air pressure with the 23 mm throttle. ....</i>	<i>62</i>
<i>Figure 5-12: Turbine pressure with the 23 mm throttle. ....</i>	<i>62</i>
<i>Figure 5-13: Air cushion surge chamber air pressure with no throttle. ....</i>	<i>63</i>
<i>Figure 5-14: Turbine pressure with no throttle. ....</i>	<i>63</i>
<i>Figure 6-1: Water flow in and out from air cushion surge chamber with 1.4 l/s discharge. ..</i>	<i>68</i>
<i>Figure 6-2: Scalar scene for downward flow with T-connection. ....</i>	<i>69</i>
<i>Figure 6-3: Pressure in front of turbine with and without a throttle with 1.4 l/s through the turbine. ....</i>	<i>71</i>
<i>Figure 6-4: Pressure in front of turbine with and without a throttle with 1.0 l/s through the turbine. ....</i>	<i>72</i>
<i>Figure 6-5: Pressure in air cushion surge chamber with 1.0 l/s discharge. ....</i>	<i>73</i>
<i>Figure 6-6: Water level in air cushion surge chamber. ....</i>	<i>74</i>
<i>Figure 6-7: Dampening effect with and without a throttled in the physical model. ....</i>	<i>74</i>

# List of tables

*Table 4-1: Physical model parameters. .... 32*

*Table 4-2: Properties for the different pipe elements ..... 36*

*Table 4-3: Main parameters for air cushion surge chamber ..... 36*

*Table 4-4: Main parameters for turbine and PID elements ..... 37*

*Table 4-5: First throttle design loss parameters from LVTrans. .... 42*

*Table 4-6: First throttle design parameters. .... 42*

*Table 4-7: Local loss coefficients ( $\zeta$ ) for the first throttle design. .... 42*

*Table 4-8: Second throttle design loss parameters from LVTrans. .... 46*

*Table 4-9: Second throttle design parameters. .... 46*

*Table 4-10: Local loss coefficients ( $\zeta$ ) for the second throttle design. .... 46*

*Table 4-11: Water velocities used in the simulations. .... 53*

*Table 5-1: Loss coefficients and loss ratios from the physical experiments with the 25 mm throttle. .... 56*

*Table 5-2: Loss coefficients and loss ratios from the 3D numerical simulations of the 25 mm throttle. .... 56*

*Table 5-3: Loss coefficients and loss ratios from the physical experiments for the 23 mm throttle. .... 59*

*Table 5-4: Loss coefficients and loss ratios from the 3D numerical simulations of the 23 mm throttle. .... 59*

*Table 6-1: Physical vs numerical loss coefficients. .... 65*

*Table 6-2: Physical vs literature loss coefficients. .... 65*

*Table 6-3: Literature vs numerical loss coefficients. .... 66*





# List of symbols

Symbol	Unit	Description
A	$m^2$	Area
b	$m$	Length of protruding pipe
c	$m/s$	Speed of sound
$C^+, C^-$	-	Characteristic lines
$C_v$	-	Local loss coefficient
D	$m$	Diameter
d	$m$	Diameter
$D_h$	$m$	Hydraulic diameter
f	-	Friction factor
g	$m/s^2$	Gravitational acceleration
H	$mWC$	Pressure height
$h_f$	$mWC$	Head loss
$h_p$	$mWC$	Pressure
i	-	Grid intersection
L	$m$	Length
m	-	Exponent for sudden contraction loss
M	-	Value in sudden expansion loss calculation
n	-	Area ratio
N	-	Value in sudden expansion loss calculation
p	$N/m^2$	Pressure
Q	$m^3/s, l/s$	Discharge
t	s	Time
$t_p$	$m$	Thickness protruding pipe
u	$m/s$	Velocity
U	$m/s$	Average velocity
v	$m/s$	Velocity
V	$m^3$	Volume
x	$m$	Distance/length
y	$m$	Distance/length
z	$m$	Distance/length
$\alpha$	$^\circ$	Angle
$\delta_1$	$m$	Protruding pipe edge
$\kappa$	-	Adiabatic constant
$\lambda$	-	Multiplier in the method of characteristics
$\nu$	$m^2/s$	Kinematic viscosity
$\zeta$	-	Local loss coefficient
$\rho$	$kg/m^3$	Mass density
$\tau_0$	$N/m^2$	Shear stress



# 1 Introduction

The scope of this master thesis is to design and build a surge tank throttle based on literature values, test this throttle in a physical model and compare the results with numerical simulations. A literature review on the throttle effects and the state-of-the-art throttle design should also be carried out as a part of the thesis. The load case for the experiments is a multiple closing and opening case to get resonance and bring the system to the maximum possible state of oscillations, which is a method used in Austria since the 1960s. The 1D numerical program LVTrans will be used to calculate the hydraulic transients in the whole system and the 3D numerical program STAR-CCM+ will be used to calculate the throttle head loss. In addition, the effects of installing a throttle in the physical model will be discussed. The physical model used in this work is a 1:65 scale model of Torpa hydropower plant constructed at the Norwegian University of Science and Technology (NTNU). This introduction chapter will describe the background for the thesis and the use of surge tanks in hydropower systems.

## 1.1 Background

Surge tanks are applied in hydropower plants for dampening of water hammer and to ensure regulation stability. In order to improve these properties, a throttle can be constructed in the connection between the headrace and the surge tank. Surge tank throttles have not been used much in Norwegian hydropower plants, but they are widely used for example in Austria.

Massive construction of wind and solar power in Europe provides increasing needs for large energy storage facilities that can utilize the unregulated power production in periods with overproduction. Hydropower pumped storage plants (PSP) are effective for storing large amount of energy, and many new PSP projects are currently under development in Austria, Switzerland and Germany.

PSPs are able to shift rapidly between pumping mode and turbine mode, which results in large hydraulic transients. Especially in PSPs with surge tanks, throttles are often applied to reduce the mass oscillations and enhance the regulation stability of the power plant. The design of the throttles is a complex process, and the throttles are designed individually for each power plant to get the best results. Due to the high development rate of new PSPs and to gain better understanding of the throttle effects, research is needed in order to further develop this technology.

### 1.2 Surge tanks

When the discharge in a hydropower system changes due to regulations of turbines, valves or pumps, elastic shock waves occur in the system. This shock wave will propagate to the nearest free water surface, and then be reflected back, and give a large interior pressure in the water conduit. To avoid damage on the system and oversizing of valves, gates, turbines and pipes, this pressure must be limited. This is done by establish a free water surface closer to the turbine (Guttormsen, 2006), either with an open surge shaft or an closed air cushion surge chamber. The introduction of a surge shaft or a surge chamber solves the problem with the water hammer, but it introduces the new problem of mass oscillations between the surge shaft and the reservoir. The mass oscillations will occur both when the discharge increases and decreases, and it will continue until the oscillations are dampened out by friction and local losses in the tunnel. The water hammer and the mass oscillations will be described in more detail in the theory chapter in this thesis.

Figure 1-1 shows the traditionally hydropower design in Norway, and the state-of-the-art design in Norway and Austria. The traditionally Norwegian layout is a low head tunnel from the reservoir and almost to a point directly above the power station, and then a pressure shaft down to the turbine and a surge shaft up to open air. The state-of-the-art design in Norway is to construct an air cushion surge chamber and a direct pressure tunnel from the power station to the inlet reservoir (Vereide et al., 2015). An air cushion surge chamber is constructed as an excavated underground rock cavern, which is filled with compressed air. The first air cushion surge chamber in Norway was built in Driva power plant, and was put into operation in 1973 (Goodall et al., 1988). Since then nine more are built in Norway, two in China and one in the USA (Hu et al., 2007).

The state-of-the-art design in Austria is a low head tunnel, and a vertical pressure shaft down to the power station. The surge tank is constructed as a throttled chamber surge tank connected to open air. The throttled chamber surge tank consists of a lower and a upper chamber, and a shaft between these two (Vereide et al., 2015). The surge tank throttle is usually situated at the transition from the lower camber to the shaft, and the upper surge chamber includes an aeration structure. This surge tank type has been the state-of-the-art design in Austria since the construction of the Kaunertal hydropower plant in 1964 (Vereide et al., 2015).

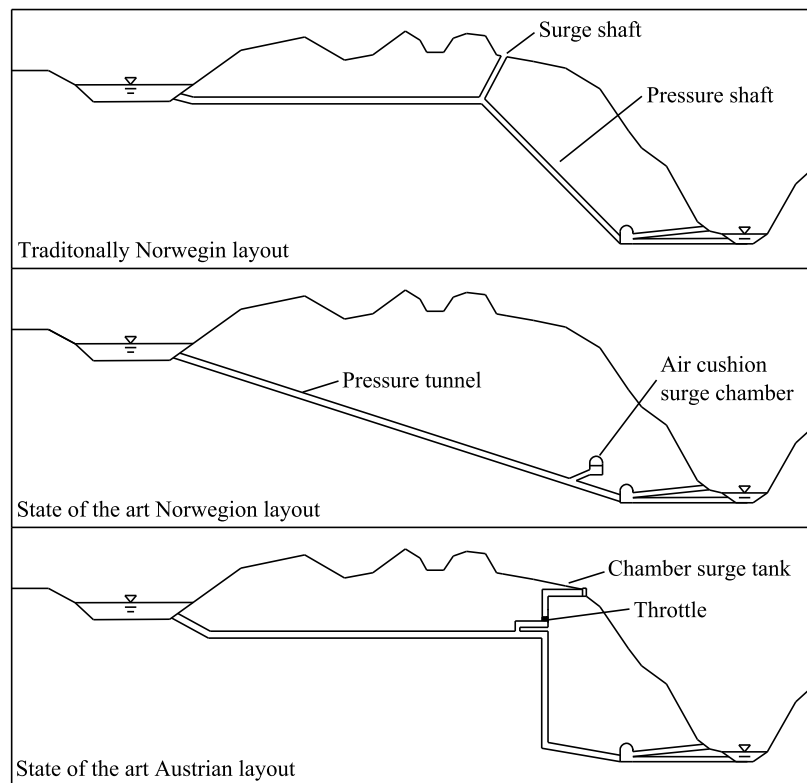


Figure 1-1: Hydropower surge tank design, modified after Vereide et al. (2015).

The different layouts have different advantages and disadvantages, and the surge tank system must be design individually for each project. For projects with problematic topography like a very high or very low overburden, the air cushion surge chamber layout is beneficial. This layout also improves the regulation stability due to a free water surface closer to the turbine. The air cushion surge chamber has more challenges with the geological conditions, and the risk of air escaping into the headrace to cause mayor blow-outs (Goodall et al., 1988). In addition, the compressors in the existing power plants have been under-dimensioned for today's requirement to minimize the down-time during inspections and work in the tunnels. For instance, the largest power plant in Norway, Kviteseid, uses 45 days to fill the air cushion after inspection (Vereide et al., 2014). The traditional Norwegian design and the Austrian state-of-the-art layout have less operational challenges, and as long as the benefits for an air cushion surge chamber is not high, these designs should be selected (Vereide et al., 2015).



## 2 Literature review

This chapter presents a literature review of the throttle effect and the state-of-the-art throttle design. Most of the articles found on the topic are from Austria, since surge tank throttles have been used in many Austrian power plants since the 1960s. In Norway, surge tank throttles are not common and little research is done on the topic. This chapter presents the findings from the literature review of surge tank throttles.

### 2.1 Surge tank throttles

Surge tank throttles are usually situated at the transition from the lower chamber to the shaft or in the connection between the headrace and the surge tank. The surge tank throttle is constructed to increase the dampening of mass oscillations in the water power system. The throttle introduces a singular loss when water is flowing in or out from the surge tank and should give a large dampening effect already in the first period of oscillations (Steyrer, 1999). The goal is to achieve a new equilibrium state as fast as possible after a change in the flow regime (Gabl et al., 2011). Especially for hydropower pumped storage plants (PSP) the implementation of a throttle is beneficial due to the massive hydraulic transients occurring in the systems. Besides giving a dampening effect, the throttle will also lower the volume demand of the surge tank and it will ensure stable and smooth operations for the machines (Richter et al., 2012b). In the Austrian layout the introduction of the surge tank throttle will decrease the volume demand for both the upper and lower chamber significantly depending on the throttle design (Steyrer, 1999). A throttle will also give a higher minimum water surface, which can be beneficial if an existing power plant has trouble with too low water surface in the surge tank. In the same way the maximum upsurge in the surge tank will be lowered. The maximum pressure in front of the turbine can also be reduced with a throttle.

### 2.2 Throttle types

Different design of the throttle will have different effects on the dampening of the mass oscillations. A throttle can mainly be designed in three different ways, which have different potentials for the ratios between upsurge and downsurge head losses. These throttletypes and the possible loss ratios are (Richter et al., 2012a):

- Symmetric throttle: 1:1
- Asymmetric throttle: 1:4
- Reverse flow throttle: 1:50

A symmetric throttle has the simplest design and it gives the same singular loss both ways, figure 2-1 shows a simple example. The asymmetric throttle is designed to give a higher loss when the water is flowing out from the surge tank, figure 2-1 shows an example of an asymmetric throttle. The reverse flow throttle (also called vortex throttle) consists of a steel torus similar to a spiral casing of a Francis turbine, shown in figure 2-1, and produces a vortex flow when water is flowing down. The water is forced to exit the torus through a small connection pipe rectangular to the plane of the vortex flow and is then flowing in to the lower chamber. This results in a very high pressure loss (Steyrer, 1999). These kinds of reverse flow throttles have earlier been used in several high head power plants in Austria, but today only the more simple asymmetric throttle is used. This is due to severe dynamic vibrations caused by the massive dissipation of energy in the reverse flow throttles (Richter et al., 2015).

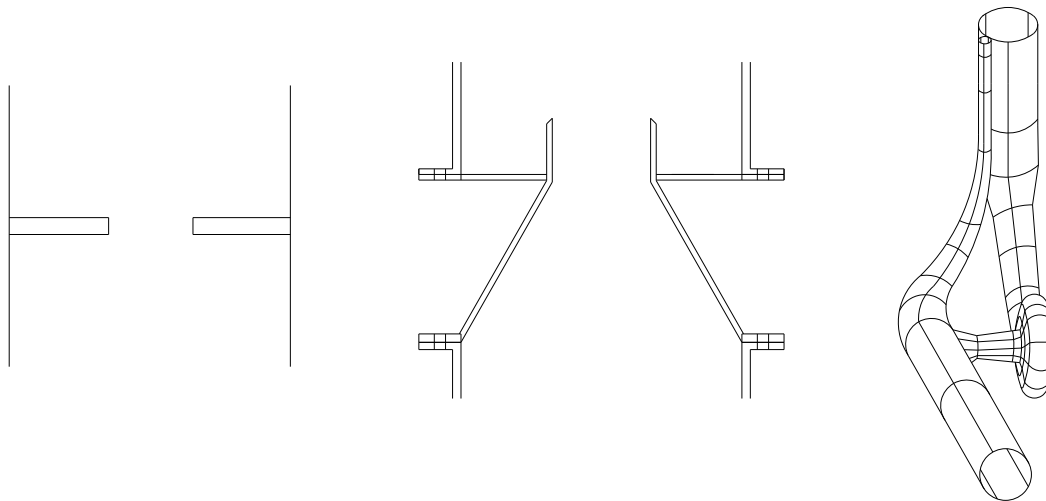


*Figure 2-1: A symmetric throttle to left, an asymmetric throttle in the middle and a reverse flow throttle (Steyrer, 1999) to the right.*

A high loss ratio can be beneficial and will give a better dampening effect. Higher throttling in upsurge direction results in an increase of the pressure head on the tunnel, but it would decrease the necessary volume of the surge tank (Richter et al., 2012a). A high loss coefficient for downward flow will give an improved dampening effect, and also a higher loss ratio. Figure 2-2 shows how the different throttle types influences on the water level and pressure in the state-of-the-art Austrian surge tank design. The figure shows how the asymmetric throttle gives a little better dampening effect than the symmetric, and the highly improved dampening effect of the reverse flow throttle.



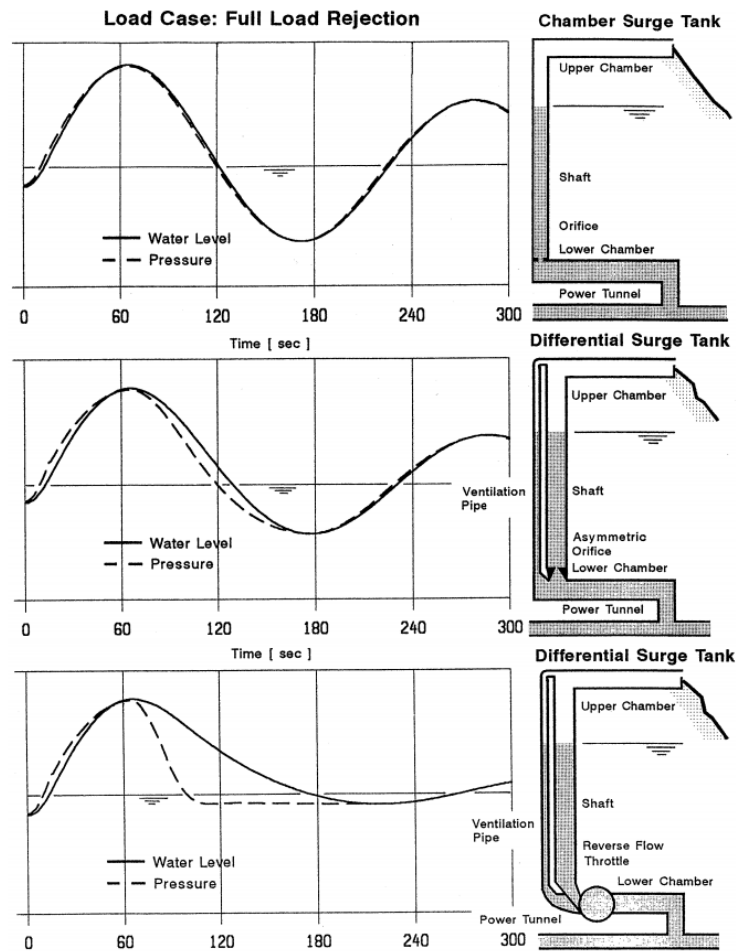


Figure 2-2: Different throttles and dampening effect (Steyrer, 1999)

The pressure in the asymmetric and reverse flow cases is controlled by the water level in the aeration shaft, which drops fast because it empties unhindered into the lower chamber. The aeration shaft is to prevent column separation in case of under pressure, which can result in damages on the main pressure tunnel (Richter et al., 2012a). More simple throttles like the symmetric and asymmetric throttles with lower ratios can be constructed without an aeration shaft. The aeration shaft should be at least one meter in diameter due to maintenance purposes (Richter et al., 2012a).

### 2.3 Throttle design process

The design of surge tank surge throttles are, as mentioned earlier, a complex process and the throttles are design individually for each power plant. There is three different methods to find the local loss coefficients (Gabl et al., 2014):

- Literature values
- Numerical simulations
- Physical model tests

A combination of all three is often used in the design process. Literature values are often used as a start, but optimization can hardly be made using only tabular values. They are normally just used as a first step before doing 3D simulations and physical model tests (Gabl et al., 2011). CFD simulations can then be used to predesign the throttle as they give the possibility of testing a large range of geometries for optimization of the throttle. Based on the numerical simulations a physical model is often constructed to test the most promising designs to verify and compare the loss coefficients. The numerical models have the advantages of flexibility, low costs (Gabl et al., 2011), and complete 3D simulations of the entire surge tank in prototype scale. However the calculations are time consuming and validation is needed (Vereide et al., 2015). The physical models on the other hand will have the advantages of less uncertainty, representation of 3D phenomena, visualization of hydraulic behavior, proving safety against outflow from aeration structures and measuring of the throttle loss. The disadvantages are no similitude for air behavior, time consumption and cost. When the loss coefficients are verified, they are applied in 1D numerical simulations to calculate the mass oscillations and water hammer behavior of the complete hydraulic system (Richter et al., 2012a).

The design load case is the worst multiple switching case, a method used in Austria since the 1960s (Richter et al., 2015). The 1D simulations are used to bring the system into the maximum possible state of oscillation, where the turbines is opened or closed near the flow amplitudes. For pumped storage plants, the mode is switched directly from turbine to pumping.

### **2.4 Asymmetric throttle design**

In this thesis, an asymmetric throttle will be designed and tested, therefore the design parameters for this type of throttle will be presented in more detail. The asymmetric throttle is chosen because this is the one used in state-of-the-art design in Austria, and it can easily be inserted in to the physical model. As described in the method chapter later, the design is relatively simple, in order to be able to build it in short time and at low cost.

The upsurge loss coefficient is determined by the tolerable pressure in the conduit system (Richter et al., 2012b). The optimal throttle design gives the lowest pressure in front of the turbine, i.e. when the water hammer pressure is equal to the mass oscillation pressure. Figure 2-3 shows the pressure in front of the turbine in a single shut down situation with an optimal throttle, a too much throttled situation and an unthrottled system. The first steep peak comes from the water hammer and the seconds wider from the mass oscillations. The optimal throttle gives a lower maximum pressure rise and appears to give an improved dampening effect, while the situation with too much throttling gives a higher pressure rise from the water hammer. The effect of the throttle on the pressure in front of the turbine and on the air pressure in the air cushion surge chamber will be further discussed in the discussion chapter.

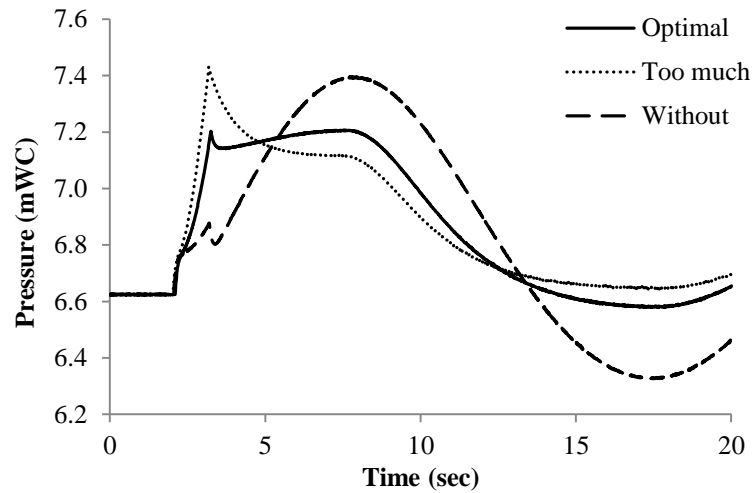


Figure 2-3: Pressure in front of turbine.

To maximize the ratio between the upsurge and downsurge loss, the throttle is design as a smooth contraction for water flowing up, and as a sudden contraction for water flowing down (Richter et al., 2012b). The optimum diameter of the contraction is the one that gives a perfect pressure development in front of the turbine. If the diameter is too small this will result in a pressure peak in front of the turbine caused by the water hammer, and if the diameter is too large this will result in a higher pressure from the mass oscillations, as seen in figure 2-3. The loss coefficient for downsurge flow is increased additionally by prolonging the contraction to make a sharp crest as seen in figure 2-4. This figure shows some of the design parameters of an asymmetric throttle design. The most important parameter is the smallest diameter for flow in both directions (Gabl et al., 2011).

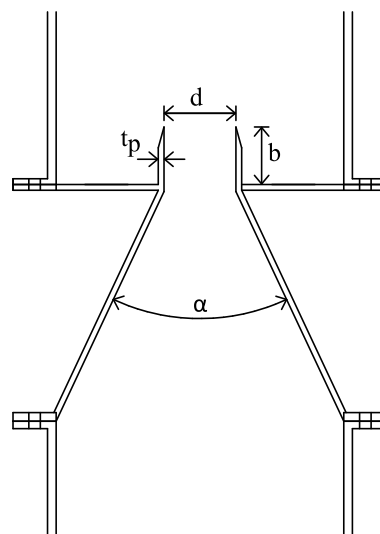


Figure 2-4: Asymmetric throttle parameters.

In the case of downward flow the length and thickness of the protruding pipe are very important for the loss coefficient, but for upward flow these parameters have little influence. When the pipe is prolonged into the shaft above, the volume of the dead space around it provides room for turbulence and cross flows during downward flow. The length of this pipe element is important to get the best effect. Idelchik (1986) gives that a length of 0.5 times the smallest diameter of the throttle is enough to get the maximum loss coefficient, and that a longer pipe element will not increase the coefficient. In Gabl et al. (2011) the maximum required dead zone length is found to be 0.4 m for a throttle with a smallest diameter of 3.0 m. Therefore, there is a little uncertainty of the required length, but no source found give any longer required length than 0.5 times the smallest diameter. In case of upward flow it has been found that the local loss coefficient is almost independent of the dead storage size (Gabl et al., 2011).

The shape of the end of the protruding pipe also has influence on the loss coefficient. There is found that by chamfering the edge at an angle of 45 degrees on the outside, the loss factor will increase with about 15 % (Richter et al., 2012b), see figure 2-5. When water flows out of the surge tank a great part of the water will have to find the exit through the orifice circulating along the wall. This circulation forces a contraction of the flow in combination with high water velocity at the center of the orifice. Instead of chamfering the edge an even thinner protruding pipe could be used and give the same results, but a minimum of steel thickness is necessary. The relation between thickness of the edge and the smallest diameter is also described by Idelchik (1986) to have a great impact on the local loss coefficient. A relatively small increase in the thickness of the edge of the protruding pipe will give a lower loss coefficient.

The converging angle of the throttle will effect the coefficients in both directions. Within the normal limits for an asymmetric throttle the losses in case of upward flow is relatively small, and in case of downward flow they are relatively high. The different losses will be described in more detail in the theory chapter.

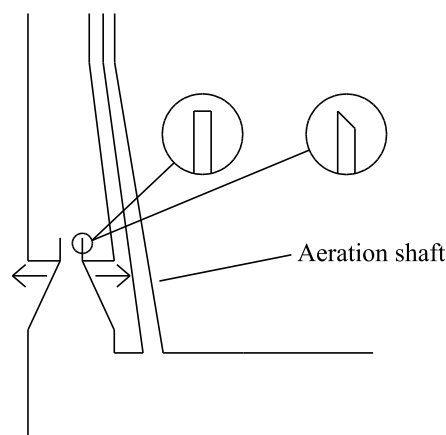


Figure 2-5: Variation in throttle design, based on Richter et al. (2012b).

Figure 2-5 shows an asymmetric throttle in the transition between the lower chamber and the shaft in a state-of-the-art Austrian layout. There has been found that there is a negligible difference in the loss coefficient by considering flow through the aeration shaft or not. But as mentioned earlier, an aeration shaft is required in case of large loss ratios to prevent column separation and damages on the system. Different positions of the throttle have also been tested and no significant influence on the loss coefficient was found (Richter et al., 2012b). The reason for testing this is because the aeration shaft is often a part of the main shaft in the surge tank, and in case of upward flow a jet will be created and this can give high dynamic forces along the concrete and steel lining. Therefore it is beneficial to place the throttle in a way that do not give high dynamic forces directly on the aeration shaft.



## 3 Theory

This chapter presents the theory behind hydraulic transients in hydropower systems. The basic equations to calculate transients in hydropower systems, and the characteristic method used to solve these equations are outlined. The different methods used to calculate the head loss in the asymmetric throttle, and the theory behind the computational fluid dynamics (CFD) modeling is also presented.

### 3.1 Hydraulic transients

Non-stationary flow conditions occur when the flow in a system changes over time, as for example due to regulation of the turbine. Under such conditions hydraulic transients like water hammer and mass oscillations will occur. In some cases the compressibility of the fluid will effect the pressure conditions, and in some cases the compressibility will be negligible. The two main types of transient flow problems in hydropower are (Guttormsen, 2006):

- Water hammer, which are elastic shock waves with a short period of a few seconds, resulting in a pressure rise in front of the turbine. Compressibility is taken into consideration.
- Mass oscillations, which are waves with a much longer period than the elastic shock waves. Compressibility is often neglected, and the fluid is considered to be incompressible.

#### 3.1.1 Water hammer

Water hammer is an elastic shock wave that occurs in closed water systems when the discharge changes due to regulations of a turbine, valve or pump. The pressure wave will propagate in the waterway, and will be reflected back when it reaches the nearest free water surface (Guttormsen, 2006). This gives a large interior pressure in the water conduit. The largest water hammer will occur during the worst multiple switching case. Especially long water systems are exposed to high pressure water hammers (Guttormsen, 2006).

Figure 3-1 shows the development of the pressure wave after a complete shutdown in a simple hydropower system. The friction and singular losses are neglected, and an instantaneous valve closing is considered. The velocity in the pipe is  $v$ , and the discharge is  $Q$ . In the end of the pipe there is a valve that is closed at the time  $t=0$  and the length from the valve to the reservoir is  $L$ . When the valve closes the water velocity just upstream the valve will be zero, and the kinetic energy will go over to potential energy in form of the pressure rise  $dp$ . This pressure wave will propagate against the reservoir with the speed  $c$ , which is the speed of

sound in water. Because of the elasticity in the water, water from the reservoir will continue to flow into the pipe.

At the time  $t = \frac{L}{c}$  the pressure wave has reached the reservoir, and it will be reflected back against the valve. At the same time the water in the pipe will run back to the reservoir due to the stored strain energy in the pipeline cannot be sustained.

At the time  $t = \frac{2L}{c}$  the pressure wave has reached back to the valve, and in this moment the pressure in the pipe is the same as before the shutdown. The water will still run back to the reservoir, and it will develop an under pressure wave travelling from the valve to the reservoir with the speed  $c$ .

At the time  $t = \frac{3L}{c}$  the water velocity in the system is zero and the negative pressure wave will be reflected back to the valve.

When  $t = \frac{4L}{c}$  the cycle is completed, and this wave oscillations will continue until the energy is dissipated by friction, which is not been considered in this simplification.

To avoid damage on the system and oversizing of valves, gates, turbine and pipes, this pressure must be limited. This can practically be done in two ways:

- slower regulation of the systems
- make the distance to the nearest free water surface shorter

To regulate the system very slow will usually be unacceptable because of requirements in the regulation of the systems, and due to loss of water. Then the only acceptable solution is to establish a free water surface closer to the turbine (Guttormsen, 2006). This can be done in two ways:

- an open surge shaft
- an air cushion surge chamber

The open surge shaft has been the traditionally way of dealing with the water hammer in Norway. This is an open shaft from the headrace tunnel and up to the surface. The air cushion surge chamber is the state-of-the-art design in Norway, and consists of a closed chamber with compressed air. The air cushion surge chamber works in the same way as a surge shaft, but with no connection to the surface. Figure 1-1 in the introduction shows the two different types.



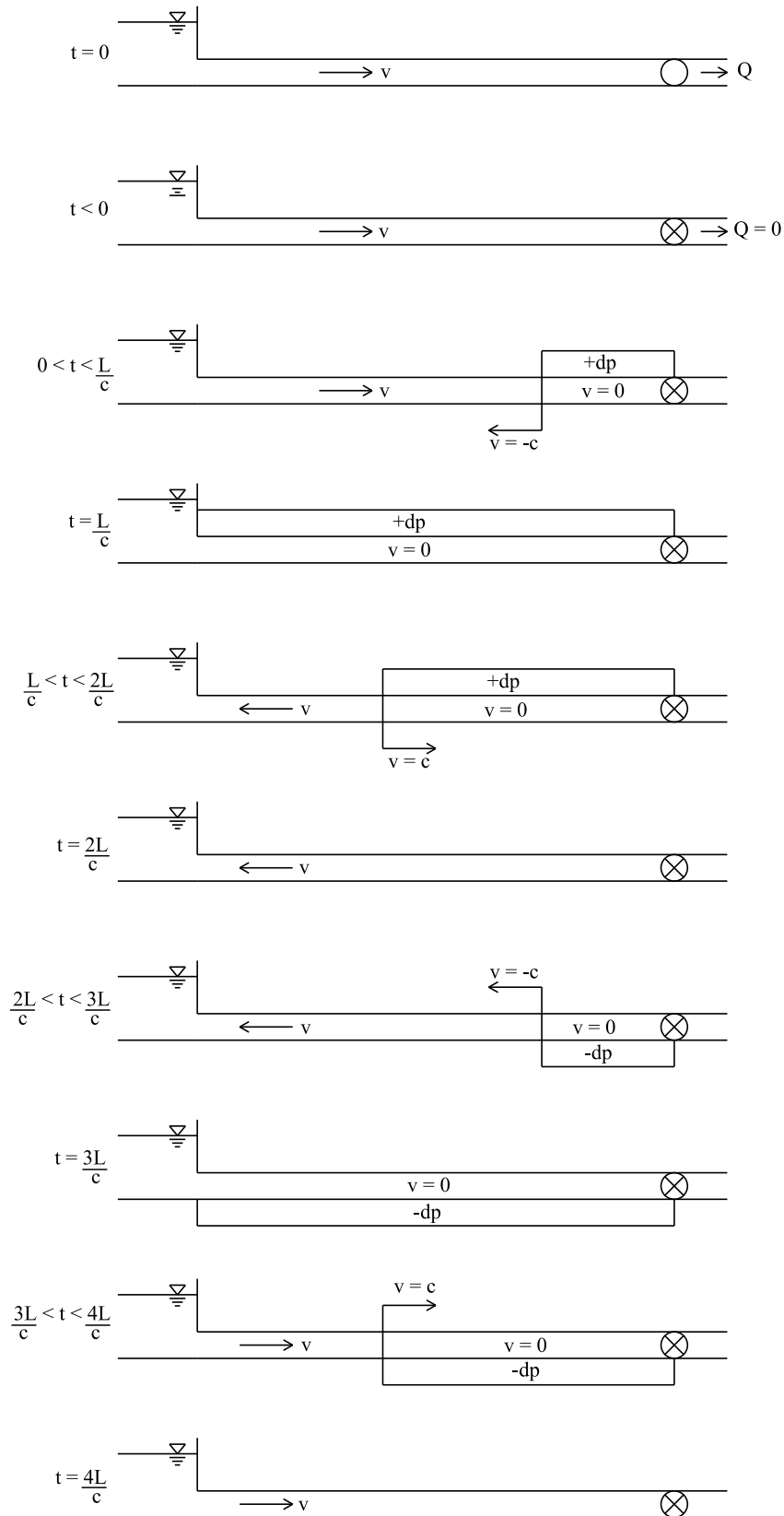


Figure 3-1: Development of water hammer, based on Guttormsen (2006)

### 3.1.2 Mass oscillations

The introduction of a surge shaft or an air cushion surge chamber solves the problem with the water hammer, but introduces the new problem of mass oscillations between the surge shaft or air cushion surge chamber and the reservoir. The mass oscillations will occur both when the discharge increase and decrease. The period of the water hammer is much shorter than the period for the mass oscillations, and it will be dampened out already when the mass oscillations are in the beginning of its development. This allows these two problems to be solved separately (Guttormsen, 2006).

Fig 3-2 shows the principle of mass oscillations for a simple power plant with a surge shaft, where the graph to the right shows the water level development in the surge shaft over time.

When the turbine is open and the discharge is stable in situation A), the water level in the surge shaft will be stable at a level  $z_0$  under the water level in the reservoir, and the system is in equilibrium. The distance  $z_0$  is due to the head loss in the in the tunnel between the reservoir and the surge shaft caused by friction and local losses (head loss will be described in more detail in chapter 3.4).

When the discharge changes, the system is no longer in equilibrium, because the head loss is no longer the same as  $z_0$ , and mass oscillations will occur. The maximum impact comes from the worst multiple switching case. The maximum water level amplitude in the surge shaft follows a closure, while the maximum downsurge will follow an opening. This example shows a single shut down situation form full discharge.

When the turbine is shut down from situation A) and if the water is considered to be incompressible, the pressure shaft is essentially plugged, and the incoming water from the reservoir will then be forced to flow up in the surge shaft. The water will rise until the pressure is high enough to stop the water masses. Situation B) shows the system at the point of maximum upsurge. The water level in the surge shaft is in this situation above the water level in the reservoir, and the water will then start to accelerate back to the reservoir.

The water level in the surge shaft has in situation C) decreased to a level below the reservoir, and the water will then flow from the reservoir and back to the shaft like in B). This will continue until the oscillations are dampened out by the friction and local losses in the tunnel.

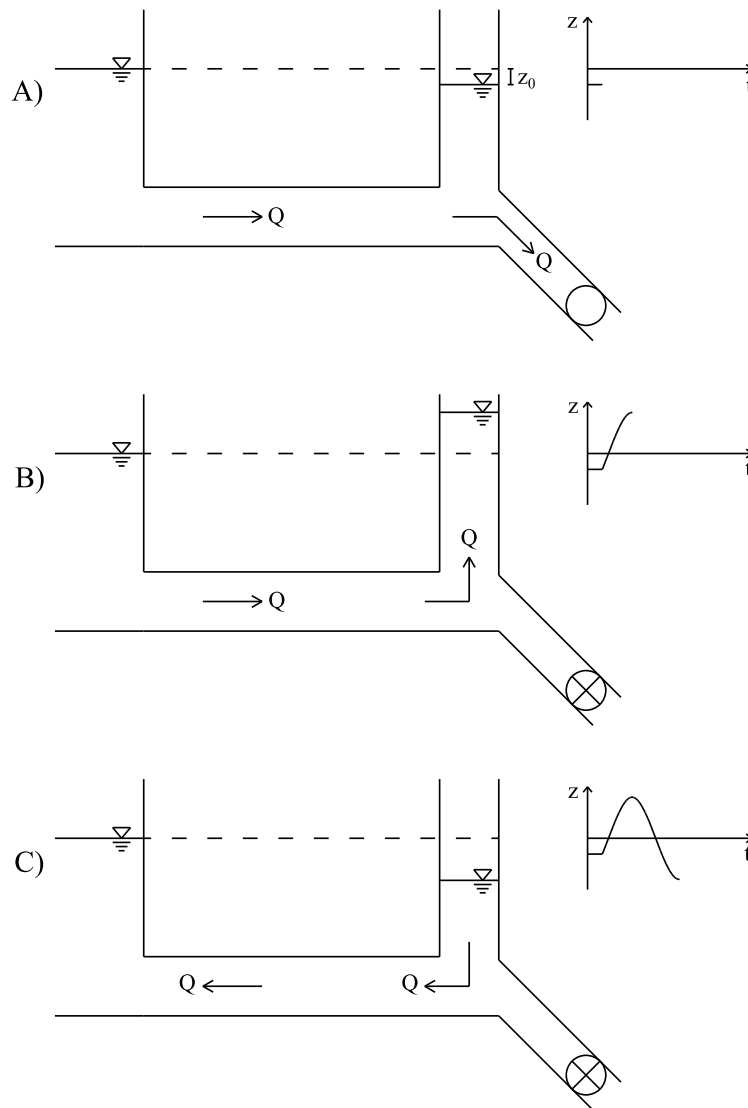


Figure 3-2: Mass oscillations in power plant with a surge shaft.

The development of mass oscillations is here shown in a system with a surge shaft, but the principle will be the same in a system with an air cushion surge chamber. When the water flows from the tunnel and in to the air cushion surge chamber like in situation B), the water level will rise until the pressure in the air cushion is high enough to stop the water masses. The water will then oscillate back and forth like described for the surge shaft.

### 3.1.3 Air cushion surge chambers

When calculating water levels in an air cushion surge chambers the assumption that the air mass in the surge tank responds adiabatically is used, and the response is then following equation 3.1 (Nielsen, 1990).

$$h_p V^K = h_{p0} V_0^K \quad (3.1)$$

This equation can then be derived with respect to  $V$ . It then gives an expression of how the air pressure in the air cushion surge chamber changes when the volume change:

$$\frac{dh_p}{dV} = \frac{-\kappa h_{p0}}{V_0} \quad (3.2)$$

Theoretical and laboratory analyses of the thermodynamics of air cushion surge chambers have concluded that the air masses would response adiabatically for typical air cushion geometries and surge periods. The adiabatic constant  $\kappa$  can then be set to 1,4 (Goodall et al., 1988).

### 3.2 Basic differential equations

The equation of motion and the continuity equation are two partial differential equation used to describe the transient flow in systems. The derivations of these two equations are found in Wylie et al. (1993).

#### 3.2.1 Equation of motion

The equation of motion is derived from a control volume shown in figure 3-3.

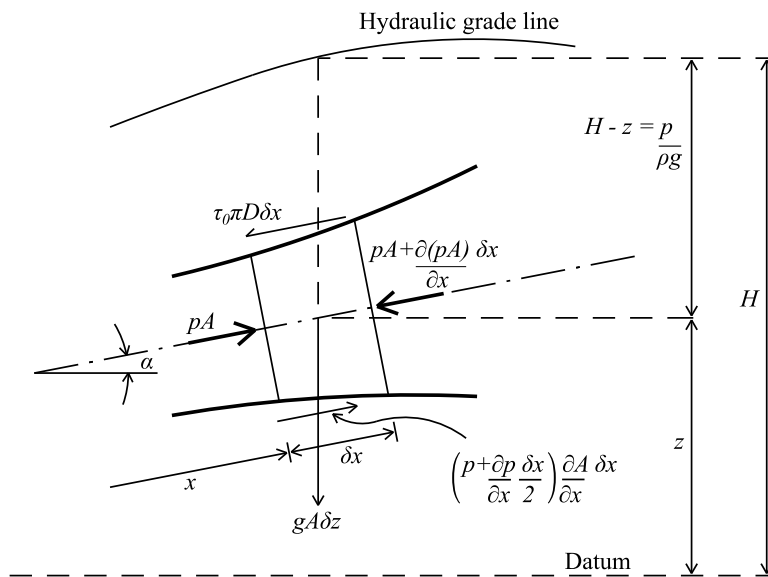


Figure 3-3: Control volume for derivation of the equation of motion. (Wylie et al., 1993)

The tube is at all times filled with liquid fluid with mass density  $\rho$ . Average pressure and velocity in the cross section are assumed. The derivation looks at equilibrium in pressure on a controll section with length  $\delta x$ , diameter  $D$  and a cross section  $A$ . The cross section is a

function of  $x$ . The tube has a small incline with a angle  $\alpha$  against the horizontal line. After some manipulation and simplification this gives the simplified hydraulic-grade-line form of the equation of motion only valid for less compressible fluids that flow with low velocity:

$$g \frac{\partial H}{\partial x} + \frac{\partial v}{\partial t} + \frac{fv|v|}{2D} = 0 \quad (3.3)$$

### 3.2.2 Continuity equation

The continuity equation is derived from a control volume shown in figure 3-4.

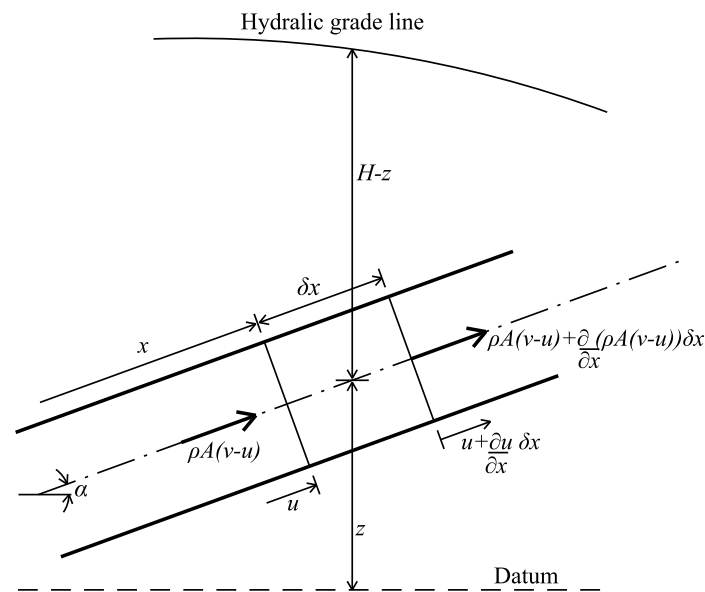


Figure 3-4: Control volume for derivation of the continuity equation. (Wylie et al., 1993)

The control volume has the length  $\delta x$ , and it moves and stretch only like the inside surface of the pipe moves and stretches. The mass law provides that the rate of mass inflow into the control volume is equal to the accumulated mass plus the mass flow out. This can be written like:

$$-\frac{\partial}{\partial x} (\rho A (v - u)) \delta x = \frac{d}{dt} (\rho A \delta x) \quad (3.4)$$

After some manipulation and simplification this gives a simplified continuity equation valid for low Mach number unsteady flow, and with the pressure replaced by the head using that  $\frac{\partial p}{\partial t} = \rho g \frac{\partial H}{\partial t}$  the equation becomes:

$$\frac{c^2}{g} \frac{\partial v}{\partial x} + \frac{\partial H}{\partial t} = 0 \quad (3.5)$$

The speed of sound comes in to the equation due to the elasticity in the water and the pipe.

### 3.3 The method of characteristics

There is no general solution of the partial differential equations that describes transient flow in systems. But by using the characteristic method this equations can be transformed into particular total differential equations that can be integrated. This gives finite difference equations, which can be solved numerically. The full derivation of the characteristic method is described in Wylie et al. (1993).

The simplified equation of motion (3.3) and continuity equation (3.5) are defined as  $L_1$  and  $L_2$ :

$$L_1 = g \frac{\partial H}{\partial x} + \frac{\partial v}{\partial t} + \frac{fv|v|}{2D} = 0 \quad (3.6)$$

$$L_2 = \frac{c^2}{g} \frac{\partial v}{\partial x} + \frac{\partial H}{\partial t} = 0 \quad (3.7)$$

By introducing an unknown multiplier  $\lambda$  equation (3.6) and (3.7) are combined to:

$$L = L_1 + L_2 = \lambda \left( \frac{\partial H}{\partial x} \frac{g}{\lambda} + \frac{\partial H}{\partial t} \right) + \left( \frac{\partial v}{\partial x} \lambda \frac{c^2}{g} + \frac{\partial v}{\partial t} \right) + \frac{fv|v|}{2D} = 0 \quad (3.8)$$

By substitution and rewriting this gives two pairs of equations, one for the positive value of  $c$ , and one for the negative value:

$$C^+ : \begin{cases} \frac{g}{c} \frac{dH}{dt} + \frac{dv}{dt} + \frac{fv|v|}{2D} = 0 & (3.9) \\ \frac{dx}{dt} = +c & (3.10) \end{cases}$$

$$C^- : \begin{cases} -\frac{g}{c} \frac{dH}{dt} + \frac{dv}{dt} + \frac{fv|v|}{2D} = 0 & (3.11) \\ \frac{dx}{dt} = -c & (3.12) \end{cases}$$

The two original partial differential equations has been converted to two total differential equation with the use of two real values of  $\lambda$ .  $C^+$  holds when the pressure wave propagating with the flow, and  $C^-$  when its propagating against the flow (Nielsen 1990). The solution can be visualized as it develops on the  $xt$ -plane. Equation (3.10) and (3.12) plots as two straight

lines as shown in figure 3-5. These two straight lines are the “characteristic lines” along which equation (3.9) and (3.11) are valid.

A pipeline is divided in an even number of parts, each with a length of  $\Delta x$ . If the variables  $v$  and  $H$  are known in A, then equation (3.9) can be integrated from A to P along the  $C^+$  line. The same can be done with equation (3.11) along the  $C^-$  line when the variables are known in B. This is resulting in two equations with the same unknown variables in the point P.

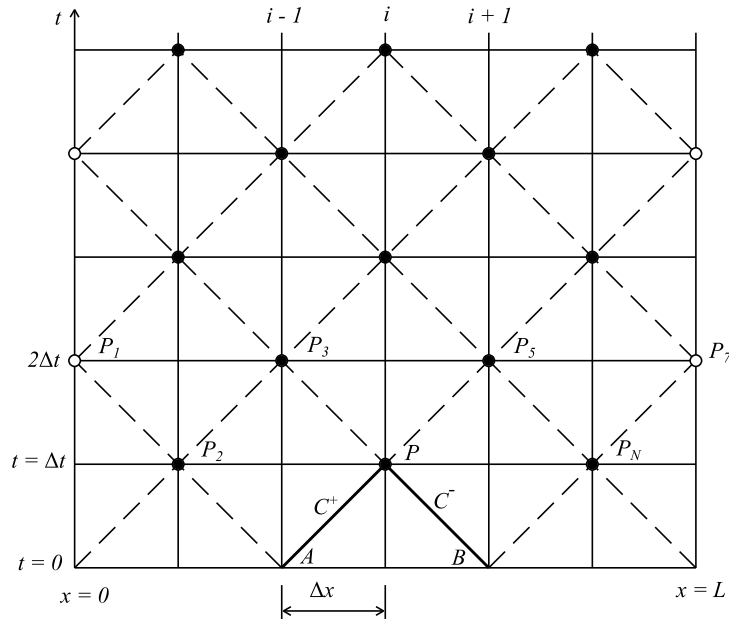


Figure 3-5:  $xt$ -network for solving the problem in simple pipes (Wylie et al., 1993).

The  $C^+$  and  $C^-$  equations are integrated along the characteristic lines, and gives basic algebraic relations that can describe the transient propagation of head and flow in a pipeline. These equations are solved for  $H_p$  and can then be written like:

$$C^+: H_P = H_A - B(Q_P - Q_A) - RQ_P|Q_A| \quad (3.13)$$

$$C^-: H_P = H_B - B(Q_P - Q_B) - RQ_P|Q_B| \quad (3.14)$$

where B is called the pipeline characteristic impedance, and is a function of the physical properties of the fluid and the pipeline:

$$B = \frac{c}{gA} \quad (3.15)$$

$RQ_P|Q_A|$  and  $RQ_P|Q_B|$  gives the friction loss over the reach  $\Delta x$ . R is the pipelines resistance coefficient:

$$R = \frac{f \Delta x}{2gDA^2} \quad (3.16)$$

The head and discharge in every iteration step can then be found by some simplification and manipulation of equation (3.13) and (3.14) as:

$$H_i = \frac{C_P B_M + C_M B_P}{B_P + B_M} \quad (3.17)$$

$$Q_i = \frac{C_P - C_M}{B_P + B_M} \quad (3.18)$$

The subscript notation used in the equations is shown in figure 3-5.  $i$  refers to any grid intersection in the  $x$  direction, and subscripted values of  $H$  and  $Q$  at each section is either given as initial conditions, or available from the preceding time step. Figure 3-5 shows that for every other time step the endpoints are used to find the solution, it is therefore important to use appropriate boundary conditions. Literature about boundary conditions can be found in Wylie et al. (1993).

## 3.4 Head loss

Head loss, or pressure loss, is loss of energy due friction and local disturbances of the water flow. In hydropower plants the local losses are usual very small compared to the friction loss, and they are therefore often neglected in more simplified estimations (Guttormsen, 2006).

### 3.4.1 Friction loss

Friction loss is caused by friction between the water and the pipe along the entire length of the pipe. The friction loss along a straight pipe with a constant cross section is calculated from the Darcy-Weisbach equation (Crowe et al., 2009):

$$\Delta p = f \frac{L}{D} \frac{\rho v^2}{2} \quad (3.19)$$

The friction factor  $f$  can be found with the Moody diagram (Moody and Princeton, 1944). Equation (3.19) can be written in terms of head loss in mWC by substituting  $\Delta p = \rho g h_f$ :

$$h_f = f \frac{L}{D} \frac{v^2}{2g} \quad (3.20)$$



### 3.4.2 Local loss

Local pressure losses are caused by changes in the pipe geometry, for example expansion, contraction, bending and valves. The local losses can be expressed with the following equation (Idelchik, 1986):

$$\Delta p = \xi \frac{\rho v^2}{2} \quad (3.21)$$

Or as head loss and mWC:

$$h_f = \xi \frac{v^2}{2g} \quad (3.22)$$

$\xi$  is a pressure loss coefficient, and values for different local loss conditions can be found in literature, for example from Idelchik (1986).

## 3.5 Local loss coefficients

The local loss coefficient for the most important processes in the asymmetric throttle design will be presented in this chapter.

### 3.5.1 Smooth contraction

Transition from a larger section to a smaller section through a smoothly converging nozzle gives irreversible loss from the total pressure. The loss coefficient depends on the converging angle and the area ratio. At large angles ( $\alpha > 10^\circ$ ) and area ratios ( $n_0 < 0.3$ ) the water will separate from the walls after the contracting section, and this is the main source of the local losses. The losses will increase all the way up to an angle of  $180^\circ$ , which will give a sudden contraction in the cross section. The local loss coefficient of a converging nozzle is given in equation (3.23) (Idelchik, 1986):

$$\xi_{loc} = \frac{(-0.0125n_0^4 + 0.0224n_0^3 - 0.00723n_0^2 + 0.00444n_0 - 0.00745)}{(\alpha_p^3 - 2\pi\alpha_p^2 - 10\alpha_p)} \quad (3.23)$$

where:

$$n_0 = \frac{A_{throttle}}{A_{pipe}} \quad (3.24)$$

$$\alpha_p = 0,01745\alpha \text{ rad } (\alpha \text{ in degrees}) \quad (3.25)$$

Within the limits  $10 < \alpha < 40^\circ$  is the resistance coefficient at a minimum, and is practically constant and equal to  $\xi = 0.05$  (Idelchik, 1986).

### 3.5.2 Sudden contraction

The flow at the entrance into a protruding pipe is depending on two relationships:

$$\text{The relativ thickness: } \frac{\delta_1}{D_h} = \frac{\text{Pipe thickness}}{\text{Hydraulic diameter}} \quad (3.26)$$

$$\text{The relativ distance: } \frac{b}{D_h} = \frac{\text{Pipe length}}{\text{Hydraulic diameter}} \quad (3.27)$$

$\delta_1$  is the thickness of the edge of the protruding pipe. The loss coefficient is at a maximum when the wall is very sharp and thin and when the pipe is at an infinite distance from the wall (in theory 0.5 times the smallest diameter). When the flow enters the pipe it separates by inertia from the inner surface close behind the entrance. The separation of the flow and the induced formation of eddies is the major source of the pressure loss. The pipe length  $b$  gives a dead storage around the protruding pipe that provides room for turbulences and cross flows which also contributes to the loss coefficient.

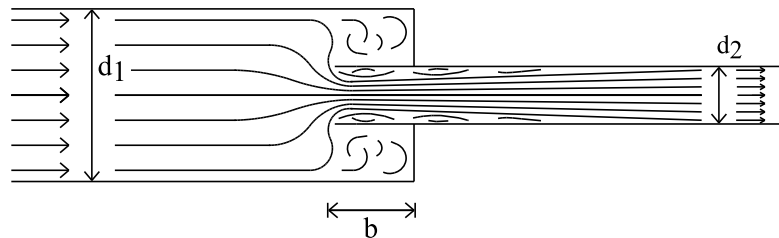


Figure 3-6: Schematic diagram of flow with a sudden contraction (Idelchik, 1986).

The local loss coefficient with a sudden contraction from a large to a small cross section is given with (Idelchik, 1986):

$$\xi = \xi' \left(1 - \frac{A_2}{A_1}\right)^m \quad (3.28)$$

$\xi'$  is a coefficient which depends on the relative thickness and distance, and is the loss coefficient used for an inlet from a much larger area (reservoir). This coefficient can be found in Idelchik (1986). The exponent  $m$  is depending on the inlet conditions and can be assumed equal to 1.0 for  $b/d_h > 0.01$ .

### 3.5.3 Smooth expansion

The local loss coefficient for a smooth expansion can be calculated with equation (3.29) (Idelchik, 1986) when the converging angle is less than  $40^\circ$ . The local losses for converging angles higher than  $40^\circ$  can be found in diagram 5-2 in Idelchik (1986).

$$\xi_{exp} = 3.2 \tan\left(\frac{\alpha}{2}\right) \left(\tan\frac{\alpha}{2}\right)^{\frac{1}{4}} \left(1 - \frac{1}{n_1}\right)^2 \quad (3.29)$$

where:

$$n_1 = \frac{A_{pipe}}{A_{throttle}} \quad (3.30)$$

With converging angles up to  $40 - 50^\circ$  the loss coefficient is smaller than for a sudden expansion, but when the converging angles is  $50 - 90^\circ$  the loss coefficient will be larger than a sudden expansion. From  $90^\circ$  the loss coefficient will drop and become close to the sudden expansion loss. Therefore there is no point to use converging angles higher than  $40 - 50^\circ$  if a minimum loss is required. For a downward flow there is beneficial to have a converging angle between  $50-90^\circ$ , to get the highest loss coefficient.

### 3.5.4 Sudden expansion

A sudden expansion of a pipe cross section area gives rise to shock waves. In an abruptly expanded section a jet is formed which is separated from the remaining medium by a boundary surface that disintegrated into strong vortices. The vortices will develop and gradually disappear while the flow will spread over the cross section in a length of 8 to  $12d_2$ . The velocity distribution upstream of an abrupt expansion is never uniform, and this substantially contributes to the losses (Idelchik, 1986).

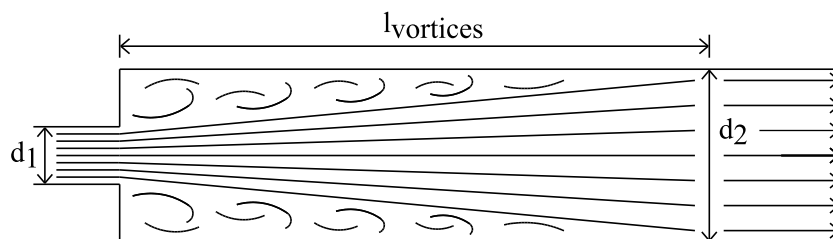


Figure 3-7: Schematic diagram of flow at a sudden expansion (Idelchik, 1986).

The local loss coefficient due to an sudden expansion can be calculated with equation (3.31) (Idelchik, 1986).

$$\xi_{loc} = \frac{1}{n^2} + N - \frac{2M}{n} \quad (3.31)$$

where:

$$n = \frac{A_2}{A_1} \quad (3.32)$$

The values of N and M can be calculated with equation (3.33) and (3.34).

$$N = \frac{(2m + 1)^3(m + 1)^3}{4m^4(2m + 3)(m + 3)} \quad (3.33)$$

$$M = \frac{(2m + 1)^2(m + 1)}{4m^2(m + 2)} \quad (3.34)$$

The factor  $m$  can vary from 1 to  $\infty$ , and is determined by the velocity profile over the cross section just upstream the expansion. At  $m = 1$ , the velocity profile has the shape of a triangle, and already from  $m = 10$  the shape is almost like a rectangle.

## 3.6 CFD modelling

Computational fluid dynamics (CFD) uses numerical methods to solve problems involving fluid flow. CFD modeling of hydraulic problems is based on solving the Navier-Stokes equations, and there are a number of different CFD programs, both commercial and free. The program used in this thesis is STAR-CCM +.

### 3.6.1 Turbulent flow

In most of the practical situations with pipe flow the flow is turbulent, which means that the flow is unpredictable with vortices, eddies and wakes. Turbulent flow occurs when the Reynold number increases, i.e. a velocity increase if the pipe is unchanged. The flow is usually (but not necessary) turbulent when the Reynolds number is larger than 4000, and when the Reynolds number is lower it is usually laminar. The Reynold number for pipe flow is given by:

$$Re = \frac{vD_h}{\nu} \quad (3.35)$$

### 3.6.2 The Navier-Stokes equations

The Navier-Stokes equations describes water velocity, and the equations are derived on the basis of equilibrium of forces on a small volume of water in laminar flow (Olsen, 2012):

$$\frac{\partial U_i}{\partial t} + U_j \frac{\partial U_i}{\partial x_j} = \frac{1}{\rho} \frac{\partial}{\partial x_j} \left( -P \delta_{ij} + \rho \nu \left( \frac{\partial U_i}{\partial x_j} + \frac{\partial U_j}{\partial x_i} \right) \right) \quad (3.36)$$

It is common to use Reynolds Averaged Navier-Stokes equations (RANS) for turbulent flow, which is Reynolds averaged versions of the equations. Figure 3-8 shows a time series of the velocity at a given location in turbulent flow.

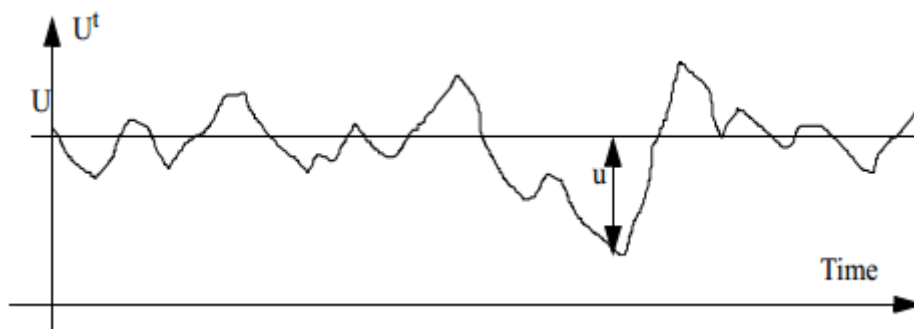


Figure 3-8: Time series of water velocity (Olsen, 2012).

The velocity is divided into an average value  $U$  and a fluctuating value  $u$ . These two variables are inserted into equation (3.36), and after some manipulation and simplification this gives the Navier-Stokes equations for turbulent flow (Olsen, 2012):

$$\frac{\partial U_i}{\partial t} + U_j \frac{\partial U_i}{\partial x_j} = \frac{1}{\rho} \frac{\partial}{\partial x_j} \left( -P \delta_{ij} - \rho \overline{u_i u_j} \right) \quad (3.37)$$

$\delta_{ij}$  is the Kronecker delta, which is 1 if  $i=j$  and 0 otherwise. The last term is the Reynolds stress term, and there are two basic approaches in STAR-CCM+ to solve this:

- Eddy viscosity models
- Reynolds stress transport models

The Eddy viscosity models use the concept of turbulent viscosity to model Reynolds stress tensor as a function of the mean flow quantities (CD-adapco, 2015). The most used model is known as the Boussinesq approximation (Olsen, 2012):

$$-\rho \overline{u_i u_j} = \rho \nu_T \left( \frac{\partial U_i}{\partial x_j} + U_j \frac{\partial U_i}{\partial x_i} \right) - \frac{3}{2} \rho k \delta_{ij} \quad (3.38)$$

$\nu_T$  is the turbulent eddy viscosity, which can be solved by several other sub models like *k-epsilon*, *k-omega* and *Spallart Allmaras*. The *k-epsilon* model will be used in the simulations in this thesis. This model solves two partial differential equations, one for the turbulent kinetic energy  $k$  and one for the dissipation rate  $\varepsilon$  (CD-adapco, 2015). The main advantage of the model is the almost universal constants, and it can therefore be used on a number of various flow situations without calibration (Olsen, 2012). The model is also a good compromise between accuracy and computational demands. Various forms of the model have been used for several decades, and it has been the most widely used model for industrial applications (CD-adapco, 2015).

Reynolds stress transport models solve the transport equations for all components of the specific Reynolds stress tensor. These models requires additional memory and computational time to be solved compared to the Eddy viscosity models, and they also require a higher number of iterations to obtain convergence (CD-adapco, 2015).

### **3.6.3 Grid**

A basic concept of CFD modelling is to divide the fluid geometry into a set of finite cells called a grid or a mesh. The Navier-Stokes equations are then solved in each cell or at the intersection between them. Grids can be classified according to characteristics like for example the structure, shape and orthogonality.

A grid can be structured or unstructured. In structured grids there is possible to identify the grids by an index, but in an unstructured this is not possible. The main advantages of an unstructured grid are that is much easier to fit the grid to the geometry, and the disadvantage is that a more complex code must be added to the solver to identify the neighboring cells.

Different cell shapes can be used when creating a grid. In a 3D grid with varying geometry it is most common to use tetrahedral, polyhedral or trimmed grid cells. Tetrahedral meshes provide an efficient solution, and are the fastest and use the least amount of memory for a given number of cells. However, there is need of approximately 5-8 times the number of cells to produce the same accuracy as with polyhedral or trimmed cells (CD-adapco, 2015). The polyhedral mesh is relative easy to fit and efficient to build, and it provides a balanced solution for complex mesh generation problems. The trimmed mesh contains of trimmed hexahedral cells that provides a robust and efficient method of producing grids for both simple and complex problems (CD-adapco, 2015). Figure 3-9 shows examples of the different shapes of cells.

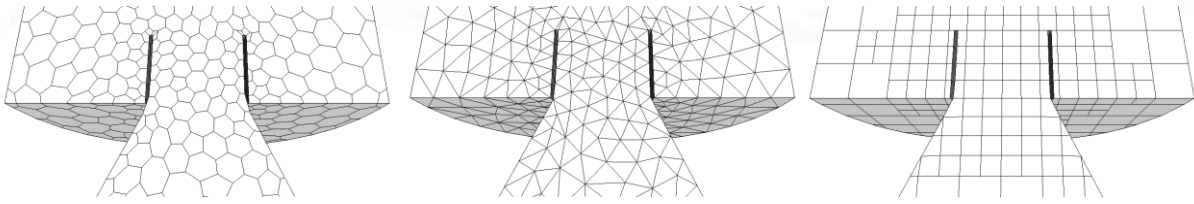


Figure 3-9: Polyhedral (left), tetrahedral (middle) and trimmed (right) meshes.

The orthogonality of a grid is determined by the angle between crossing grid lines, and if all angles are 90 degrees the grid is called orthogonal. If some crossing lines are different from 90 degrees, the grid is non-orthogonal. If the angles are below 45 degrees or over 135 degrees, the grid is said to be very non-orthogonal. High orthogonality leads to more rapid convergence and in some case better accuracy (Olsen, 2012).

Other characteristics used to define the quality of grids are the aspect and expansion ratio of the grid. The aspect ratio is the ratio between the cells lengths in x, y and z direction, while the expansion ratio is the size difference between neighboring cells. Neither the aspect ratio or the expansion ratio should be too great, in order to avoid convergence problems and inaccuracies (Olsen, 2012).

### 3.6.4 Discretization

Discretization is to transform a partial differential equation into a new equation where the variables in one cell are a function of the variables in the neighbor cells. The new function can be thought of as a weighted average of the neighboring cells (Olsen, 2012). Discretization can be illustrated with a two dimensional situation, where the concentration in the middle cell should be found.

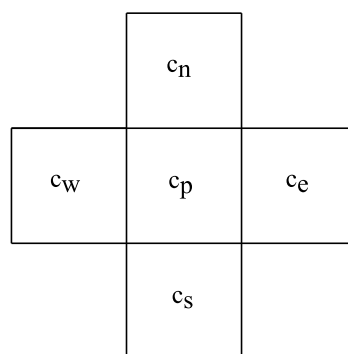


Figure 3-10: Two dimensional discretization molecule.

The formula for the concentration in the middle cell becomes (Olsen, 2012):

$$c_p = \frac{a_w c_w + a_e c_e + a_n c_n + a_s c_s}{a_p} \quad (3.39)$$

The notation refers to the directions north, south, east and west, the  $a$ -factors are weighting factors for the different cells and  $c$  is the concentration in each cell. The weighing factor for the middle cell is the sum of the neighboring weighing factors ( $a_p = a_e + a_w + a_n + a_s$ ). There are a number of different discretization methods, for example the first order upstream scheme and the second order upstream scheme (Olsen, 2012).

### **3.6.5 Boundary conditions**

Boundaries are surfaces that completely surround and define a region. It is necessary to set some boundary conditions to get a closed set of equations that can be solved from the Navier-Stokes equations (Olsen, 2012). Examples of boundaries are:

- Inflow boundary
- Outflow boundary
- Wall boundary

There is also possible to split the fluid geometry in half and define a symmetry plane. This represents an imaginary plane of symmetry in the simulation, which can be beneficial to use to save computational power and make the simulations go faster.

### **3.6.6 Convergence**

The solution method of the RANS equations is an iterative process. The principle is to guess a starting value for the variables and then iterate to find the solution. To decide if the solution has converged a criteria is selected, usually based on the residuals. The residuals are a measure of the difference between the correct values and the values in the current iteration. Low residuals indicates that the solution is converging (Olsen, 2012).



## 4 Method

This chapter describes the models and the methods used in the thesis. It includes a description of the physical model and how it is used, a description of the setup and calibration of a 1D numerical model of the system and the 3D numerical modeling of the surge tank throttle effect.

### 4.1 Physical model

The physical model used in this thesis is a 1:65 scale model of Torpa hydropower plant constructed at NTNU.

#### 4.1.1 About the physical model

The physical model is a part of a research program at NTNU, which has been initiated to gain better understanding of the physical properties of air cushion surge chambers, and to further develop the design of these constructions. The general layout of the model is presented in figure 4-1.

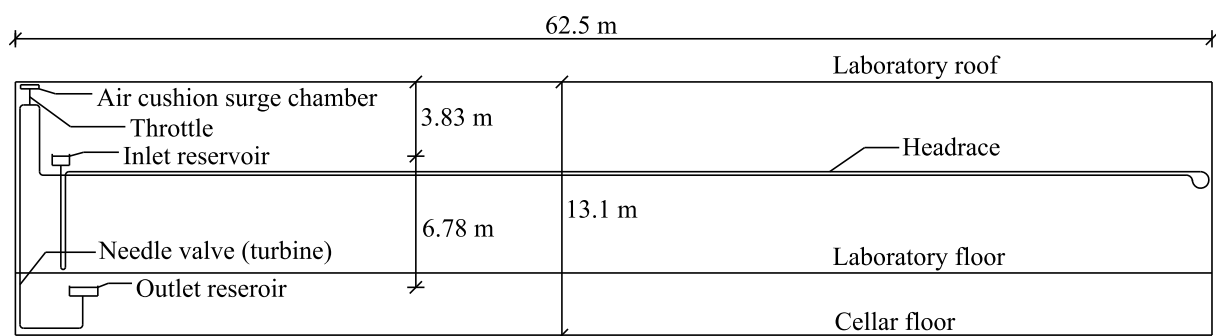


Figure 4-1: Physical model layout.

The water conduit is constructed of stainless steel pipes and the air cushion is constructed in plexiglass. The turbine is simulated with a needle valve, and in the connection pipe between the headrace and the air cushion it is possible to mount a throttle. The main dimensions of the model are presented in table 4-1.

Table 4-1: Physical model parameters.

Part	Dimension	Unit
Scaled discharge from prototype	0.001	$m^3/s$
Headrace length	148.0	$m$
Headrace diameter	0.10	$m$
Surge chamber volume(total)	0.065	$m^3$
Air pressure, absolute	6.51	$mWC$
Turbine closing time	1.25	$s$
Upper reservoir level	6.88	$m$
Lower reservoir level	0.10	$m$

As can be seen in figure 4-1, the air cushion surge chamber is placed at a higher elevation than the inlet reservoir. This is to obtain the correct relation between pressure and water level. This results in incorrect pressures for major parts of the model compared with the prototype, but the pressure in vital points, like the air cushion and in front of the turbine, is confirmed to be correct (Vereide et al., 2014). In these vital points there are mounted pressure gauges. There are mounted pressure gauges five places, where three are directly used in the thesis. These are the pressure gauges in the air cushion surge chamber, in the top of the shaft and in front of the turbine. The gauge in top of the shaft is located 1.15 meters under center of the highest part of the headrace tunnel, while the gauge in front of the turbine is located 0.43 meters above the turbine (valve). In addition, there are also two gauges in the headrace tunnel. The water system of the model is shown in the sketch in figure 4-2.

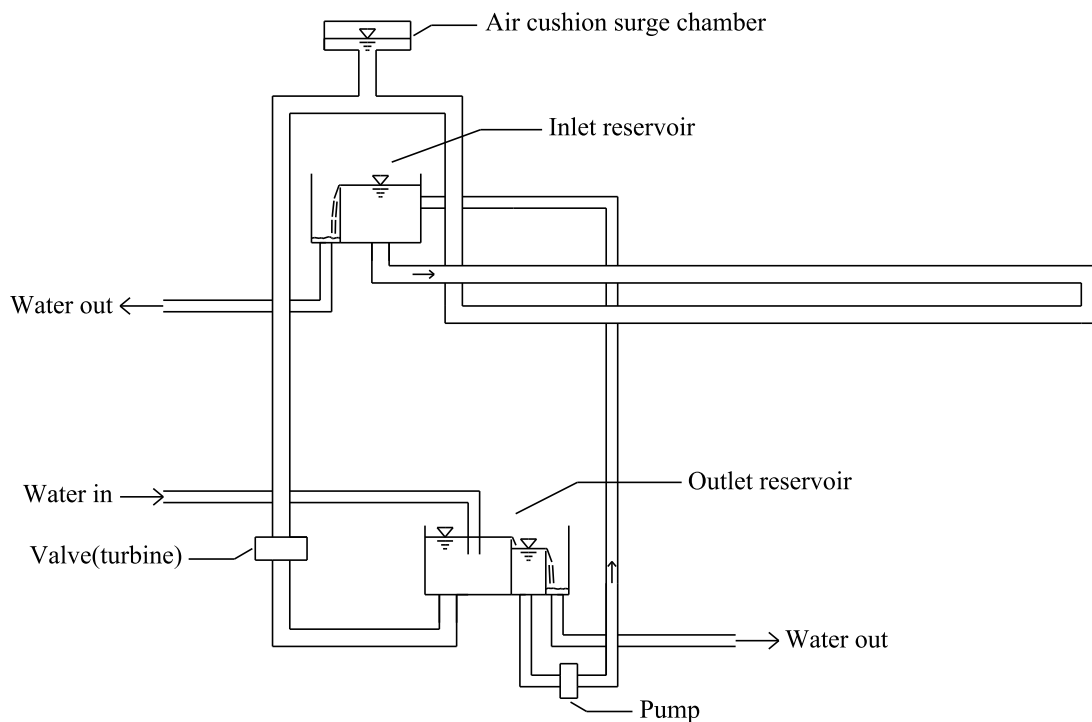


Figure 4-2: The physical model water system.

The water is flowing into the outlet reservoir of the model from the public water system. From the outlet reservoir the water flows over a weir to a pumping chamber, where water is pumped up to the inlet reservoir. Overflow water from the pumping chamber is collected in a third chamber where the water flows out of the model and back to the public system. The inlet reservoir also has the possibility of overflowing, which happens when the water amount pumped up to the reservoir is larger than the amount used in the system, or the valve is closed. This water will also flow back to the public system. From the inlet the water flows through the system and down to the outlet reservoir. During operation the water amount in the system is usually smaller than the amount pumped into the inlet reservoir to keep constant pressure, but in shorter time periods the discharge in the system is increased above the pumping discharge. This is done to flush out air before experiments, or to run model tests with higher discharge for a limited time.

#### **4.1.2 About the model tests**

After the model has been drained it is important to run the model for a long time before starting experiments, in order to flush air trapped in the model. The model is run for a couple of working days after draining, most of the time with approximately 1.0 l/s, but for periods with higher discharge to drag out even more air.

Before conduction an experiment in the physical model after it has not been used for some time, it is important that the model runs for some time to ensure that the water and pipes gets the same temperature, as the temperature may affect the pressure gauges. The necessary time is controlled with the help of the two pressure gauges in the headrace. Shortly after starting the model the pressure in these two gauges will not be parallel and linear during stable conditions, but after some time these will be parallel and linear and experiments can then be conducted.

The load case for the experiments is a multiple closing and opening case to get resonance and bring the system to the maximum possible state of oscillations. Experience in Austria has shown that three switching (closed-open) operations are enough to get convergence, so this is used in the thesis. It is important to perform the switching at the correct time, to maximize the resonance. In the physical model the timing is controlled by watching the pressure development in front of the turbine, and open/close the turbine with the experience from the 1D simulations. After an experiment the discharge in the connection pipe between the headrace and the air cushion surge chamber is calculated to check if the closing and opening of the turbine was done with correct timing.

The discharge in the connection pipe between the air cushion and the headrace is not measured in the model, so this must be calculated by the pressure change in the air cushion. This can be done with equation (3.2) from the theory chapter. The area of the water surface in the air cushion is known and is constant since the air cushion is a rectangular box, and the adiabatic constant is set to 1.4. Then the change in air volume is calculated for every time step, and then also the discharge in and out from the air cushion can be found.

## 4.2 1D simulations of the system

The 1D numerical model used in this thesis is performed with the simulation software LVTrans. In this part LVTrans will be briefly presented, and then the model will be presented in more detail.

### 4.2.1 *LVTrans*

LVTrans (Lab View Transient Pipe Analysis) is a 1D simulation software for flow in pipe systems. It is especially designed for water power systems and most of the elements are design for this purpose. The characteristics method, which is described in the theory chapter, is used to solve the partial differential equations that describe transient flow in systems. These partial differential equations were also described earlier (the equation of motion and the continuity equation). This gives an approximately analytical exact solution and the method is very quick (Svingen, 2007).

LVTrans uses LabVIEW (Laboratory Virtual Instrument Engineering Workbench) as graphical interface and it is object based. Different elements represents different parts of the power plant, such as constant water levels upstream and downstream, pipes, turbines etc. The elements are described separately and then connected together. Every element that is not a pipe must be connected to a pipe element. The elements are then given input parameters, such as diameter, lengths, friction factors, loss coefficients etc.

The source code of LVTrans is open and editable, so it is possible to change and create new elements. But for a general hydropower power plant there is no need for this, since all the elements are already made (Svingen, 2007). It is possible to make changes in the system all the time while the simulation is running. The simulation results can be seen as graphs for each element, and it is possible to log the desired one.

### 4.2.2 *Model overview*

The layout of the numerical model used in this project is shown in figure 4-3, with a total of 12 elements. The inputs for the different elements are described in more detail later in this chapter.

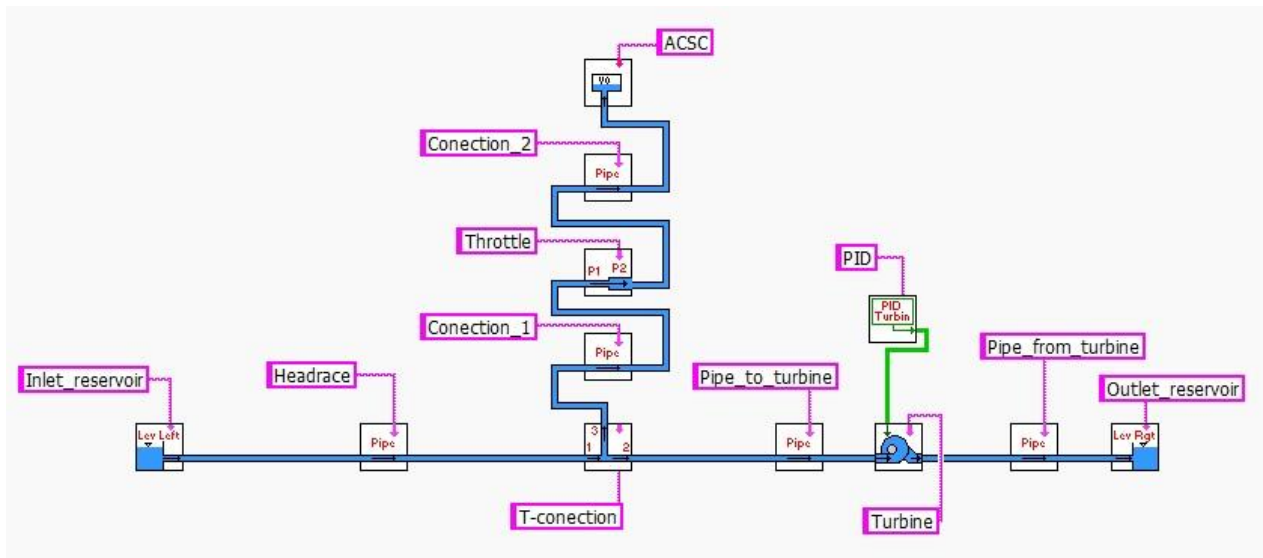


Figure 4-3: 1D numerical model overview.

### 4.2.3 Model input

Many of the elements require input parameters for total pressure  $H_0$  and the discharge  $Q_0$  under stable conditions. These values are used as starting values in the simulations, and they have only impact on how long time the system needs to stabilize. The system will adjust to the input data for the other elements like the inlet reservoir, outlet reservoir and turbine.

The factor  $C_v$  is used in LVTrans for local losses, and it is often mentioned as  $C_{vp}$  and  $C_{vm}$ . Where  $C_{vp}$  is flow in normal direction and  $C_{vm}$  is flow against normal direction. The equation for  $C_v$  is (Svingen, 2007):

$$C_v = \frac{Q_0^2}{2H_0} = \frac{A^2 g}{\xi} \quad (4.1)$$

Where  $\xi$  is the same friction factor mentioned in the theory and can be found in literature or by calibration to known data.

Some of the local losses are included in the friction loss in the pipes and the friction factor in the pipes is therefore a little bit larger than in reality. The friction factor is also the same as described in the theory.

#### Reservoirs

The water levels in the inlet and outlet reservoir are given in table 4-1 in the physical model chapter. The loss coefficients are kept unchanged and the head loss is included in the friction loss in the pipes.

#### Pipes

All the pipes are made of stainless steel with an inner diameter of 0.1 m. The properties for the different pipes are shown in table 4-2, and figure 4-3 shows where they are located in the

model.  $Z_0$  is the starting elevation of the pipe above datum, and  $Z_1$  is the end elevation above datum. Datum is placed in the center of the turbine.

Table 4-2: Properties for the different pipe elements

Pipe element	L (m)	$Z_0$ (m)	$Z_1$ (m)
Headrace	147.00	6.50	9.65
Pipe_to_turbine	9.93	9.65	0.00
Pipe_from_turbine	7.12	0.00	-0.50
Connection_1	0.21	9.65	9.86
Connection_2	0.67	9.86	10.53

### Air cushion surge chamber

The air cushion surge chamber in the physical model is a rectangular box made of plexiglass, where the inside dimensions are 1.00m x 0.43m x 0.15m. The initial air pressure in the air cushion is found from the physical model experiments, but the water level in the air cushion surge chamber must be calculated. This is done with the following relationship:

$$z_{inlet\ reservoir\ water\ level} + P_{inlet} = z_{air\ cushion\ water\ level} + P_{initial\ air\ cushion} \quad (4.2)$$

The outside air pressure is also very important to change in the numerical model before every experiment when comparing the physical and numerical model. This is measured at the same time as the physical model experiments for each experiment. The adiabatic constant must also be specified in the air cushion surge chamber parameters, and this is set to 1.4 as mentioned earlier. The main parameters of the air cushion surge chamber used for the calibration are presented in table 4-3.

Table 4-3: Main parameters for air cushion surge chamber

Parameter	Value	Unit
Initial water level	10.57	<i>m above datum</i>
Initial air pressure	6.52	<i>mWC</i>
Outside air pressure	10.21	<i>mWC</i>
Initial air volume	0.045	<i>m<sup>3</sup></i>

### Turbine and PID

The PID unit is connected to the turbine and this is the regulator that regulates the turbine. The most important input for the turbine is the design head and discharge, and for the PID unit this it is the closing time. These values are the same as for the physical model, and the values used for the calibration are shown in table 4-4. The rest of the input parameters are found with a excel sheet that comes with the program, but they are not presented here. This because they have no significance other than gets the model to run stable, because there is no turbine, just a valve.

Table 4-4: Main parameters for turbine and PID elements.

	Value	Unit
Discharge	0.00125	$m^3/s$
Design head	6.78	$mWC$
Closing time	1.4	$s$

The scaled closing time from the prototype gives the closing time to be 1.25 seconds in the physical model, with a discharge of 1.0 l/s. In the physical experiments different discharge is used by changing the valve opening. This means that the closing time is not always 1.25 seconds. The closing time used in the numerical model with varying discharges is shown in equation (4.3).

$$t_{closing} = \frac{1,25 \times valve\ opening}{45} \quad (4.3)$$

This is because 1,0 l/s gives a valve opening of 45%.

### **T-connection**

The headrace and the connection pipe to the air cushion surge chamber are connected with a T-connection, as shown in figure 4-3. It has one loss coefficient for each part, but these are all kept unchanged, and the loss is included in the friction loss of the pipes.

### **Throttle**

The throttle element has one local loss coefficient for upward flow and one for downward flow. These values are set to the default settings in the calibration, where there is no throttle in the model, and are later changed to find the throttle loss coefficients.

#### **4.2.4 Calibration**

When the model is set up with all the initial values and information as described, it has to be calibrated. This is done by comparing the numerical model with a physical model experiment with no throttling and a single full shutdown situation.

The friction coefficient in the pipes is found by trial and error and is kept the same for all pipe elements. The pressure in the air cushion and in front of the turbine during steady state is used to calibrate the model. The friction factor is found to be 0.11. The high friction factor is because there are high singular losses in the pipes due to bends and valves. Figure 4-4 shows the pressure development in the air cushion after a single full shutdown, and the pressure development in front of the turbine is shown in figure 4-5.

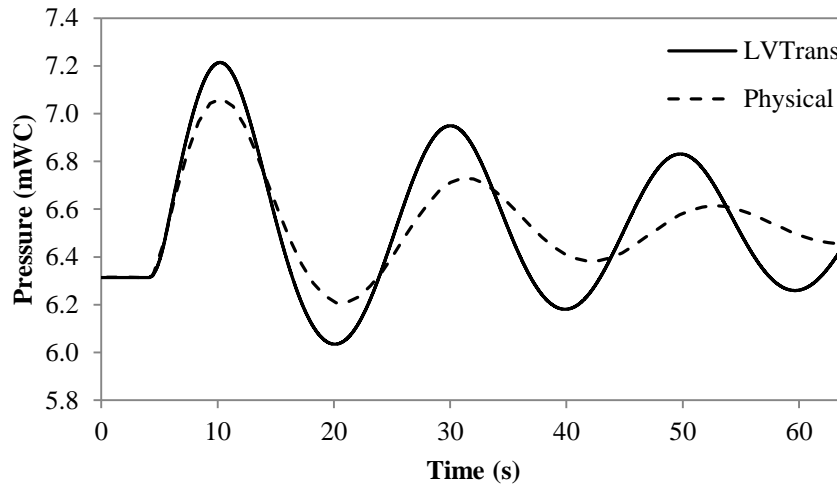


Figure 4-4: Pressure in the air cushion surge chamber.

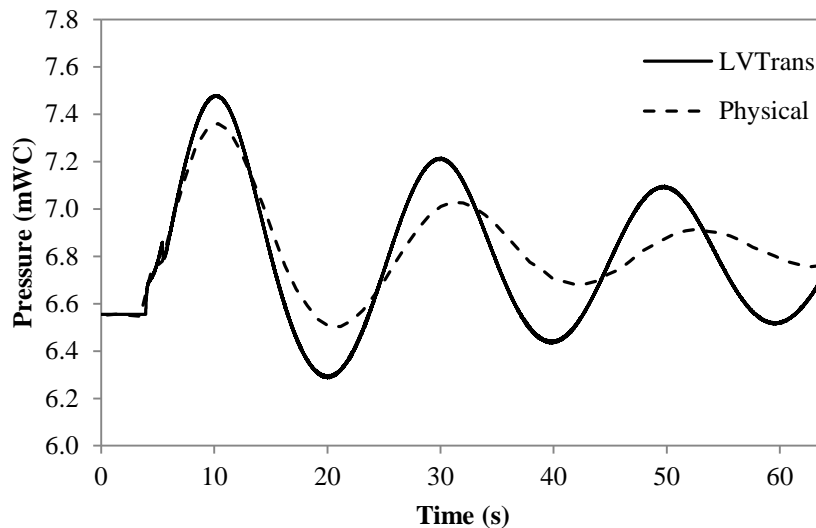


Figure 4-5: Pressure in front of the turbine.

It is important for the calibration of the model to notice that the gauge in front of the turbine is located 0.43 m above the valve that simulates the turbine, and take this in to the calculations of the pressure in front of the turbine.

As can be seen, the physical model has higher dampening than the numerical model. This is most probably caused by the non-stationary friction losses which are not properly represented due to the friction model in the equation of motion. In the equation of motion the friction losses are calculated with Darcy-Weisbach equation with the speed expressed like:

$$v^2 = v|v| \quad (4.4)$$

The simplifications assume the friction loss under unstable conditions to be the same as the friction loss under steady conditions with the same discharge, and the absolute sign gives the friction force to always be in the opposite direction than the water velocity. Figure 4-6 A)



shows how this simplification looks like in principle when the flow turns from one direction to the other. The velocity profile is in reality more like in 4-6 B) when the flow turns from one direction to the other. The figure shows that the numerical model will have too little dampening effect compared to the physical model (Nielsen, 1990).

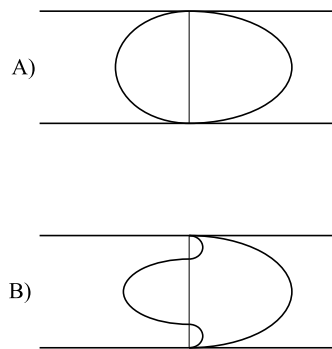


Figure 4-6: Velocity profiles in pipes when the flow turns around (Nielsen, 1990).

The period is also a little bit different, and it has been found that the period in the numerical model is constant with 20 seconds, while the period in the physical model varies between 21 and 23 seconds. This can possibly be explained by the conditions in the inlet reservoir in the physical model. This is pretty small and has the opportunity of overflowing, which is shown in figure 4-2. When the water oscillates in to the inlet reservoir, the water level will rise a little and it will flow over. This may give some errors in the period, and also give a higher dampening effect. If this water level rise is scaled up it is too large compared to the prototype. The water level is usually assumed to be constant in calculations due to the size of the reservoirs. Another factor that can affect the period is the possibility of air in the physical model. This could give reduced cross sections that influence the period, and the dampening in the model. Air in the model may also cause significant head loss and capacity reduction. This explains why there is so important to run the model for a long time prior to experiments to flush air.

#### 4.2.5 About the simulations

The load case for the simulations is a multiple switching case, as for the physical model experiments. In LVTrans it is possible to monitor the elements, and this is done with the pipe element between the headrace and the air cushion surge chamber in order to open and close the turbine in the right time. There is also possible to pause the simulations. This makes it much easier to get correct timing in the numerical simulations than for the physical model tests. The time step is set to 0.001 seconds for both the calculation and the logging. This is to ensure all details to be captured in both the calculations and the logs.

The most important elements are monitored and logged, and afterwards the data is exported to Excel for post-processing. These include the turbine, the connecting pipe, the headrace and the air cushion surge chamber. The log from the connection pipe is used to determine the

timing of the opening and closing and to find the water flow in this pipe for use in the 3D numerical simulations of the throttle effects. The headrace log is used to verify the discharge and the air cushion surge chamber gives the air pressure in this place.

### 4.3 Physical modelling of the surge tank throttle

The 1D numerical model of the whole system was used to find the loss coefficients for the throttle that gave the optimal turbine pressure. These values were then compared with literature values. The factors  $C_{vp}$  and  $C_{vm}$  are used to describe the losses in LVTrans, and equation (4.1) shows the relationship with the factor  $\xi$  which is found in literature. The throttle is made of plexiglass and then tested in the physical model. Due to an error in the first LVTrans calculation, the first throttle was designed with a too large discharge. The results from these experiments were used in the design of the second throttle, and to compare the literature values with the numerical and physical model tests. The error caused the throttling to be designed with a larger diameter than what was optimal for the model.

#### 4.3.1 Throttle parameters

The throttle design is an asymmetric throttle and the geometry is kept relatively simple, so it would be possible to construct it without practical problems. The main parameter for the throttle design was found to be the smallest diameter ( $d$ ) of the throttle. In the design process this was kept on a millimeter precision to make it possible to create as designed. The other parameters that were found to have impact on the throttling and were used in the design, were the converging angle ( $\alpha$ ), the protruding pipe length ( $b$ ) and the protruding pipe shape ( $t_p$  and edge shape). These parameters are shown in figure 4-7.

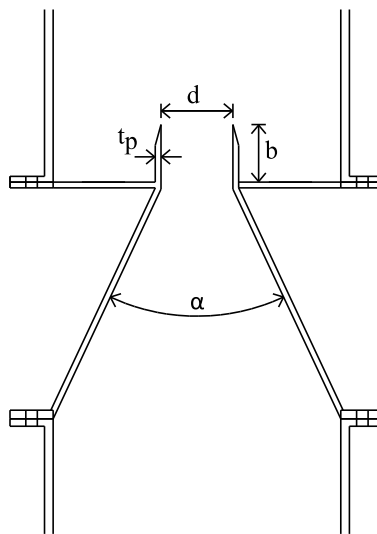


Figure 4-7: Throttle parameters

The local loss coefficient for the throttle was divided into two parameters in each flow direction. In the upward flow the local loss was divided into a smooth contraction followed by a sudden expansion. For upward flow a simplification was made by not considering the volume of the dead space around the protruding pipe. This simplification is believed to have minimal impact, and it has been found that the local loss coefficient for upward flow is almost independent from the size of the dead zone. For the downward flow the actual geometry of the throttle was used to determine the local loss coefficient, and the loss coefficient was divided into a sudden contraction followed by a smooth expansion. Figure 4-8 shows the simplified geometry and the actual geometry used to find the local loss coefficients.

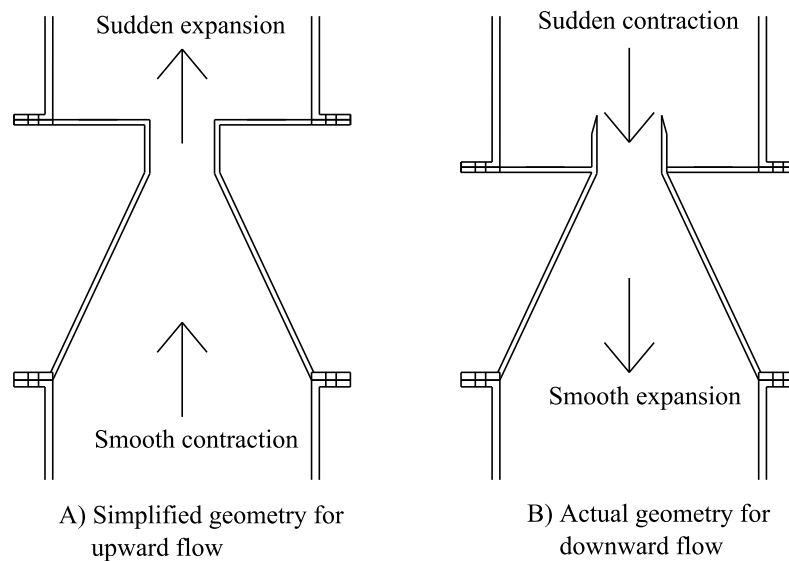


Figure 4-8: Simplified and actual throttle geometry.

The equations and theory used to calculate the different losses are described in the theory chapter, but some choices were made:

- The length of the protruding pipe ( $b$ ) could according to literature be set to  $0.5d$ , and any increasing of the length would not influence on the sudden contraction loss. This length was set to 20 mm for both throttles that were made just to ensure the dead storage to be large enough since a little increment should not have any negative impact on the loss coefficients. This choice also made the throttle easier to build.
- The value  $m$  in the sudden expansion calculation was set to 10. This corresponds to an almost rectangular velocity distribution at the sudden expansion section. At the inlet through a smooth entry or collector, the water velocity profile would be uniform (Idelchik, 1986) and therefore a value of 10 is used, since this indicated an almost uniform velocity profile. This parameter is most important when the value is small, which is typical for laminar flow, but already from about 8-10 this indicated an almost rectangular velocity profile, and the solution would be approximated constant.

- A converging angle of  $50^\circ$  was used. According to the theory this should be a good compromise between minimum loss in upward direction and maximum loss in downward direction, to get a high ratio between downsurge and upsurge losses.

### 4.3.2 First throttle design

The first throttle was designed for a discharge of 1.8 l/s, which was more than intended, but an error in LVTrans gave a higher discharge. But the throttle and the throttle effects will still be used in the comparison of the different methods, as mentioned in the introduction to this chapter. The 1D numerical model of the whole system gave the loss coefficients in table 4-5 to be optimal for the pressure in front of the turbine. The losses are related to the water velocity in the pipe under and above the throttle:

Table 4-5: First throttle design loss parameters from LVTrans.

Flow direction	$C_v$	$\xi$
Upward	$2.36 \times 10^{-6}$	257
Downward	$1.56 \times 10^{-6}$	389

The throttle was designed with the dimensions shown in table 4-6, where the different parameters are shown in figure 4-7.

Table 4-6: First throttle design parameters.

Parameter	Dimension	Unit
Smallest diameter, d	25	mm
Converging angle, $\alpha$	50	$^\circ$
Pipe length, b	20	mm
Pipe thickness	Thin as possible	mm

The literature values for the different local losses with the parameters from table 4-6 are shown in table 4-7. The loss coefficients are related to the water velocity in the pipe under and above the throttle.

Table 4-7: Local loss coefficients ( $\xi$ ) for the first throttle design.

Local loss	Upward flow	Downward flow
Contraction	24	163
Expansion	233	226
Total	257	389

The ratio between the upsurge and downsurge loss coefficient from the literature values was 1.52. The throttle was built as shown in figure 4-9. The protruding pipe was made with a length of 25 mm, which is 5 mm more than intended, but this is supposed to have minimal effect on the results. This will just give a little larger dead storage when the water is flowing downward. The protruding pipe was made 2 mm thick and approximately 0.6 mm at the edge.

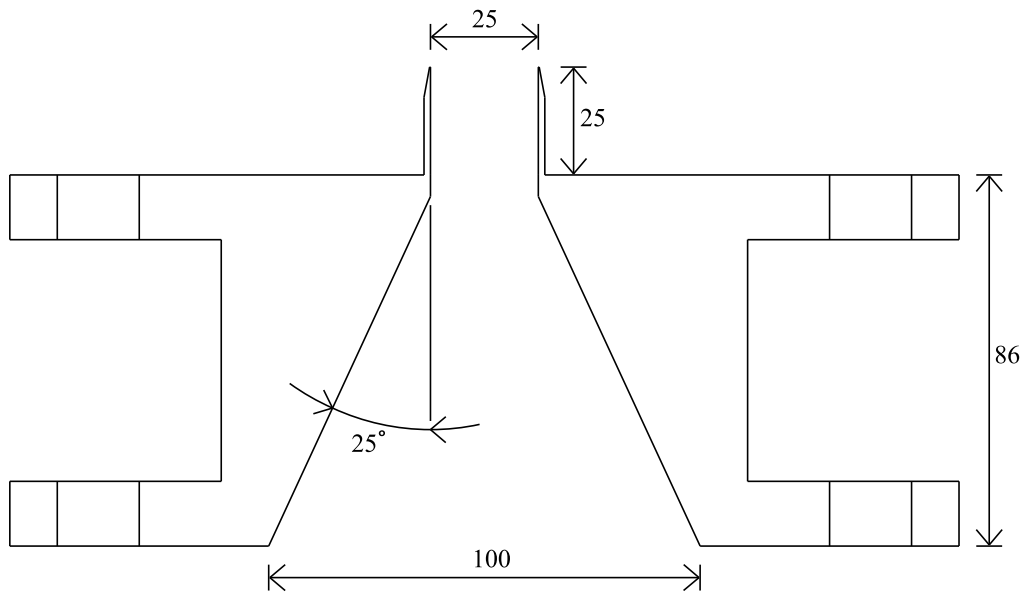


Figure 4-9: First throttle design as built.

Figure 4-10 shows a photograph of the first throttle design made with plexiglass. The throttle is made out of four pieces of plexiglass, and the division of the throttle is shown in figure 4-11. Figure 4-12 shows a close up photograph of the protruding pipe, and figure 4-13 show the throttle when it is mounted in the system.



Figure 4-10: Photography of the first throttle design.

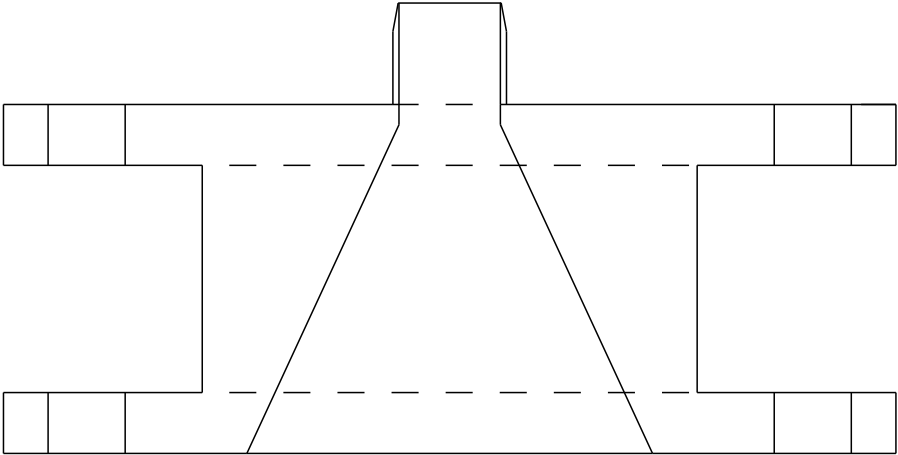
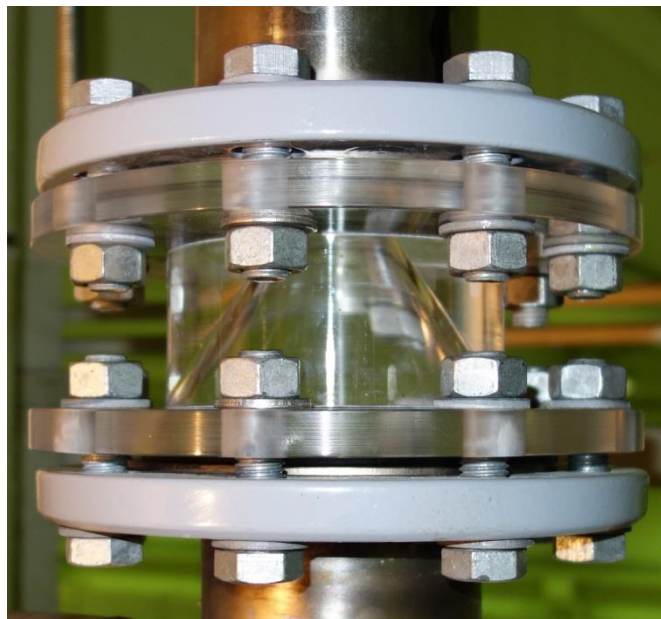


Figure 4-11: Construction pieces of the throttle.



*Figure 4-12: Detail photograph of the smallest diameter.*



*Figure 4-13: First throttle mounted in the physical model.*

### **4.3.3 Second throttle design**

The second throttle was designed in the same way as the first throttle, but the experiences from the first throttle were used to improve the design. The first throttle design gave a perfect pressure development for a discharge of 2.3 l/s in the physical model, and when this was recreated with LVTrans the literature values gave to little effect. LVTrans gave a perfect pressure in front of the turbine with literature values of a 24 mm throttle with a discharge of 2.3 l/s. The second throttle was designed for a discharge of 1.0 l/s, and due to the results from

the first throttle the second throttle was designed 1 mm larger than the results from LVTrans indicated. Table 4-8 shows the upward and downward loss coefficients the throttle was design for, where the losses are related to the water velocity in the pipe under and above the throttle.

Table 4-8: Second throttle design loss parameters from LVTrans.

Flow direction	$C_v$	$\xi$
Upward	$1.66 \times 10^{-6}$	364
Downward	$9.76 \times 10^{-7}$	620

The dimensions of the throttle are presented in table 4-9, and the parameters are shown in figure 4-7.

Table 4-9: Second throttle design parameters.

Parameter	Dimension	Unit
Smallest diameter, d	23	mm
Converging angle, $\alpha$	50	°
Pipe length, b	20	mm
Pipe thickness	Thin as possible	mm

The only parameter that is changed from the first throttle design is the smallest diameter, which is 2 mm smaller than in the first throttle design. As mentioned before, this parameter is the most important for the total loss coefficient in both directions. The literature values for the different local losses are shown in table 4-10. The losses are related to the water velocity in the pipe under and above the throttle.

Table 4-10: Local loss coefficients ( $\xi$ ) for the second throttle design.

Local loss	Upward flow	Downward flow
Contraction	33	305
Expansion	331	315
Total	364	620

Figure 4-14 shows the second throttle as built. The only difference from the first is the smallest diameter, and the throttle is also 3 mm higher due to the decrease in the diameter and the same converging angle. The protruding pipe was made 1 mm thin and approximately 0.2 mm at the edge, so it was both thinner and sharper than the first throttle. The ratio between the upsurge and downsurge loss coefficient from the literature values was 1.70 for this throttle. The increase is due to the thinner and sharper protruding pipe.



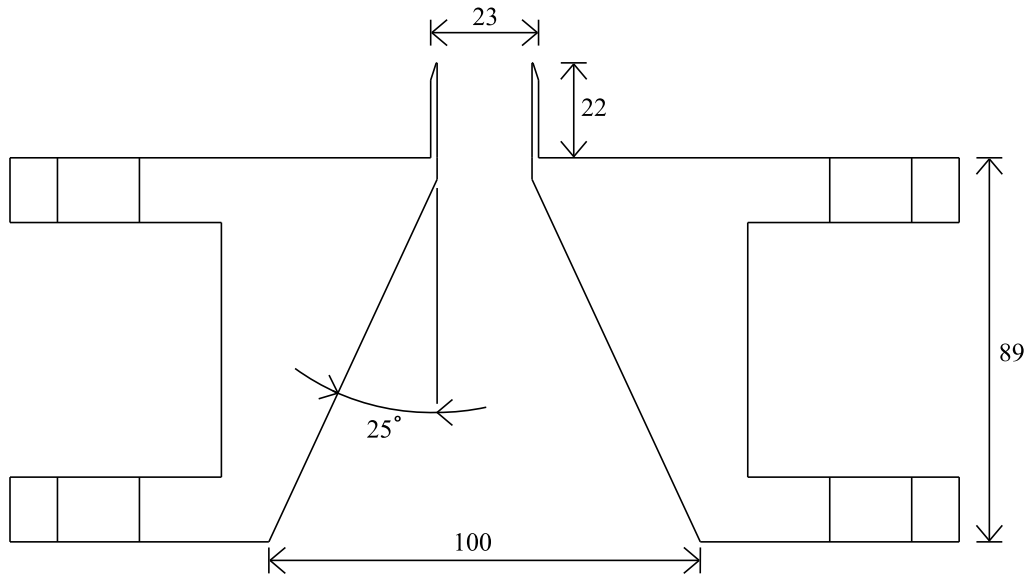


Figure 4-14: Second throttle design as built.

Due to the small changes there are no photos of the second throttle, and the throttle was also built in the same way with four pieces of plexiglass.

#### 4.3.4 Local loss coefficient calculations

The local head loss in the throttle was calculated with the pressure gauge in the air cushion and the pressure gauge in top of the pressure shaft down to the valve. The pressure different between the two gauges was plotted, and then the pressure different under stable conditions were subtracted from the maximum or minimum pressure difference to find the pressure loss caused by the throttle. Next, the corresponding water velocity was used to calculate the head loss with equation (3.22) from the theory chapter. The water flow was calculated with respect to the pressure change in the air cushion as described in the method about the physical model. The loss coefficients were calculated at the time with maximum water flow in or out from the air cushion surge chamber. The experiments were conducted with a sample frequency of 1000 Hz, and in order to obtain an acceptable accuracy in the post processing plots the log was set to 500 samples per mean, which gives a time step in the plots of 0.5 seconds.

Each throttle was tested with four different discharges for each method to see if they were constant or varied with different discharges in the system. These discharges was the maximum scaled discharge from the prototype of 1.0 l/s, the discharges that gave the optimal pressure development for the two different throttles, and one in the middle of these two. The first tests of the throttles in the physical model were conducted to find the optimal discharges, and then the four discharges were determined, and both throttles were tested for all four. It was also conducted experiments with no throttle in the system for all four system discharges to determine the loss between the two pressure gauges in an unthrottled system.

The friction loss is neglected for all calculations, and in case of downward flow the velocity height is neglected. Both these simplifications are assumed to have negligible effect on the results due to small values.

### 4.4 3D simulations of the throttle effects

The numerical simulations of the throttle are done in STAR-CCM+, and the geometries are made in AutoCAD Civil 3D. In this part the methods for the simulations will be presented.

#### 4.4.1 Geometry

The fluid geometries are made in the program AutoCAD Civil 3D, which is a commercial software application developed and marketed by Autodesk. In both ends of the throttling a pipe with length of  $15d$  is added to ensure uniform velocity distribution on the points of measuring the pressure loss. In the theory it was found that the vortices developing after a sudden expansion will gradually disappear while the flow will spread over the cross section in a length of 8 to  $12d$ , which means that  $15d$  will be enough to ensure stable conditions. When the geometry is finished it is cut in half to make the computations faster with the help of a symmetry plane. When the fluid geometries are finished in Civil 3D, they are exported as stereo lithography files (.stl files), that can be imported to STAR-CCM+. This file format only describes the surface geometry of a three-dimensional object, without any representation of the color texture or other common CAD model attributes (CD-adapco, 2015).

#### 4.4.2 STAR-CCM+

STAR-CCM+ is a commercial CFD program that includes a 3D-cad modeler, meshing tools, multiple CFD models and post-processing tools. The program is design to solve problems involving flow, heat transfer and stress. It is an object-oriented program, and an object tree is provided for each simulation, containing object reports of all data associated with the simulation.

#### 4.4.3 Mesh

The making of mesh in STAR-CCM+ includes a surface mesh and a volume mesh. To make a mesh a 3D file has to be imported or made in the included 3D modeler. STAR-CCM+ has two choices for making the surface mesh (CD-adapco, 2015):

- Surface Remesher
- Surface Wrapper

The surface remesher is used to improve and triangulate the overall quality of an existing surface and optimize it for the volume mesh models. This is done when the imported surface

is closed but composed of bad quality triangles, for i.e. .stl data. Surface wrapper is an option that can be used when the imported surface is of poor quality with intersecting surfaces, holes or gaps. The result is not necessary of optimal quality, so it usually used with the surface remesher to provide a higher quality (CD-adapco, 2015).

The fluid geometry is imported to STAR-CCM+ as a .stl file, so the imported surface has a closed surface, but the quality is not good and suitable for simulations. The surface remesher is selected and the base size of the mesh is set to 0.01 m. Figure 4-15 shows an example of a surface mesh before and after the surface remesher has been used on an imported .stl file.

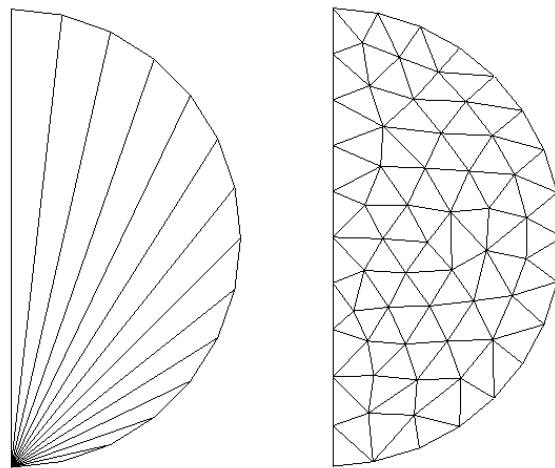


*Figure 4-15: Imported surface to left and remeshed surface to right.*

The surface mesh is used as a starting point for generating the volume mesh. The different volume mesh models available in STAR-CCM+ are (CD-adapco, 2015):

- Tetrahedral
- Polyhedral
- Trimmed
- Thin mesh

The first three are described in the theory, and the last one is a mesher used to generate a prismatic volume mesh for thin regions. The polyhedral volume mesher is chosen in the simulations in this work. This mesher is relatively easy and efficient and produces the same accuracy as a tetrahedral mesh with approximately five times fewer cells for a given surface (CD-adapco, 2015). The base size is the same as was defined for the surface mesh with 0.01 m.

In addition to a polyhedral volume mesh a “prism layer mesher” model is chosen. This is a model used to generate orthogonal prismatic cells next to wall surfaces or boundaries. This is necessary to improve the accuracy of the flow solution. This layer is defined by its thickness, number of layers and stretching. The prism layers allow the solver to resolve near wall flow accurately such as separation. Depending of the Reynolds number, a turbulent shear layer

requires 10-20 cells in the cross-stream direction for accurate resolution of the turbulent flow profiles (CD-adapco, 2015). The prism layers also reduce the numerical diffusion near the wall. The default setting is used for the thickness and stretching, but the number of prism layers are improved to 25. This gave a noticeable improvement of the residual plot. Figure 4-16 shows a corner in a volume mesh with polyhedral cells and a prism layer with two layers.

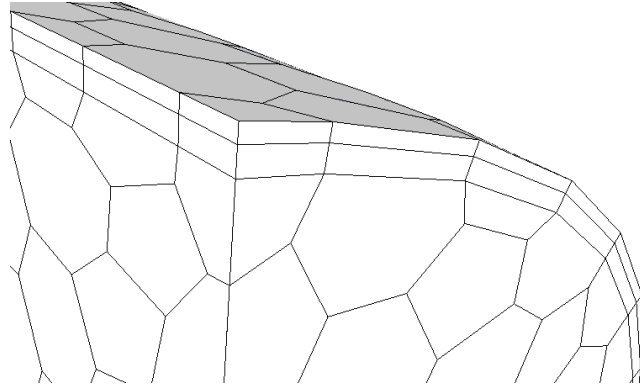


*Figure 4-16: Polyhedral volume mesh with prism layer with two layers.*

There is also possible to specify the mesh density in a specific zone for both the surface and the volume mesh with a volumetric control. This makes it possible to make a finer grid in critical areas. In these simulations this was done in the zone where the jet from the throttle where formed. Figure 4-17 shows the volumetric control boxes that were used for both upward and downward flow. The size of the grid cells in the volumetric controls can be set to a percentage of the base size, or it can be set to an absolute value. In these simulations it was set to 25 percent of the base size, which gives it an absolute size of 0.0025 m. The prism layer properties must also be specified, and they are chosen to be the same as for the rest of the volume mesh with 25 prism layers and default values on the other parameters.

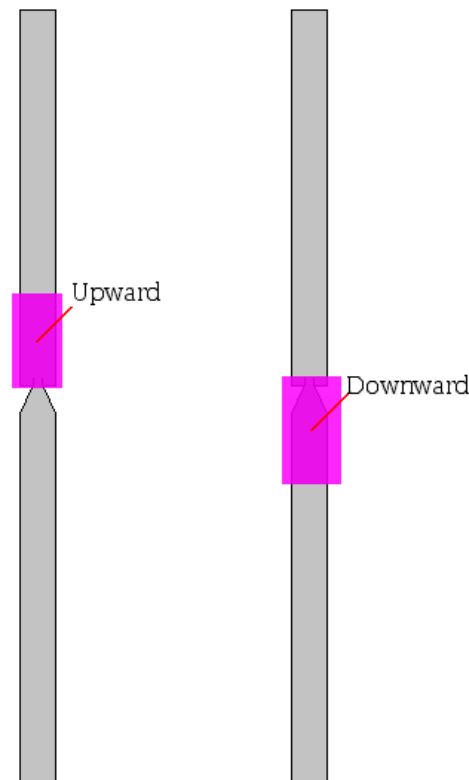


Figure 4-17: Volumetric control boxes for upward and downward flow.

#### 4.4.4 Physics

The following choices were made under the physical model selection:

- **Time:** Implicit unsteady
- **Material:** Liquid
- **Flow:** Segregated flow
- **Equation of state:** IAPWS-IF97 (water)
- **Energy:** Segregated fluid isothermal
- **Viscous regime:** Turbulent
- **Turbulence method:** RANS equations are automatic selected for turbulent flow
- **Turbulence model:** K-epsilon turbulent model

An implicit method is a method where the dependent variables are defined by coupled sets of equations and an iterative method is used to obtain the solution. In CFD the governing equations are nonlinear and the number of unknown variables is typically very large, and under such conditions implicit formulated equations are almost always solved using iterative techniques (CD-adapco, 2015). The time step in the implicit unsteady solver is set to 0.01 seconds in the simulations.

The equation of state models are used to compute the density and density derivatives with respect to temperature and pressure (CD-adapco, 2015). The IAPWS-IF97 (International

Association for the Properties of Water and Steam, Industrial Formulation 1997) allows running the simulations with liquid water. These models include calculations of density and other thermodynamics properties.

The segregated flow model solves the flow equations in an uncoupled manner. The model is used in constant density flow, but can also handle mildly compressible flow. The segregated fluid isothermal model keeps the temperature in the continuum constant, and can be used in problems where the temperature variation are small or can be neglected. It would be computationally expensive to solve an ordinary transport equation when it would yield a nearly constant field of temperature (CD-adapco, 2015).

The Reynolds number for the flow is calculated with equation (3.35) from the theory. A discharge of 1.0 l/s in the system corresponds to a water velocity of 0.13 m/s. The Reynolds number is then calculated to be approximately 13 000, which means that the flow is turbulent and a turbulent flow viscous regime is chosen.

The RANS equations are automatic selected when the turbulent flow regime are chosen. The “Auto-select recommended physical models” is a function in the physical modeling selection that allows the program to select the recommended models. Also when the *K-epsilon* turbulent model is chosen, the program automatic adds two other recommended sub models. The RANS equations and the *K-epsilon* model are both presented in the theory chapter.

### **4.4.5 Boundary conditions**

The surface is divided with the “Split part surfaces by angle” function, and then a boundary is created for each surface part. Each boundary has a corresponding node in the simulation tree, and its own properties. The boundaries used in the simulation and their properties are:

- Velocity inlet: The velocity is specified as an input value, and this is found from the 1D simulation in LVTrans.
- Pressure outlet: The pressure is specified as an input parameter, and this is found from the physical model tests. The pressure was set to the same in both directions. This was confirmed to not have any effect on the loss calculations by doing a test with changed pressure in the downward direction.
- Symmetry plane: The geometry is cut in half, and this plane is defined as a symmetry plane represents an imaginary plane of symmetry in the simulation.
- Walls: Represent an impermeable surface. All other boundaries are walls. The default setting of the wall surface is smooth. This setting is kept in order to find the pressure loss caused by the throttle.

### **4.4.6 Post-processing**

STAR-CCM+ has several post-processing tools to monitor and analyze the simulation during and after it is done. The following tools were used during and after the simulation:

- Residual plot
- Scalar scenes
- Vector scenes
- Pressure drop plot

The residual plot is created automatically, and is useful to monitor during the simulations to see how good the simulations run, and how fast it converge. The scalar and vector scenes were used to visualize the simulations.

It is possible to make reports that provide summaries of solution data. A report of the pressure drop between the velocity inlet and the pressure outlet has been created. There is also possible to make a plot of the report and then monitor it during the simulation and export it to Excel when the simulation is stopped. A pressure loss plot has been used to calculate the loss coefficient of the throttle.

#### 4.4.7 Loss coefficient calculations

The water velocity used as an input parameter in the simulations is found from the 1D numerical model, and the pressure in the outlet boundary are found from the physical model and kept the same for water flow in both directions. Table 4-11 shows the water velocities before and after the throttle used in the simulations.

Table 4-11: Water velocities used in the simulations.

Discharge (l/s)	23 mm		25 mm		Unit
	Upward	Downward	Upward	Downward	
1.0	0.16	0.15	0.17	0.16	<i>m/s</i>
1.4	0.19	0.18	0.20	0.19	<i>m/s</i>
1.9	0.22	0.20	0.24	0.22	<i>m/s</i>
2.3	0.24	0.21	0.26	0.23	<i>m/s</i>

The pressure at the top and the bottom of the throttle was exported to excel, and the head loss was found. The local loss coefficients were calculated with equation (3.22) as for the physical model experiments. The stopping criteria for the simulations were set to 1000 iteration steps, which give 2.0 seconds in physical time.





## 5 Results

This chapter presents the results from the physical model experiments and the numerical simulation of the throttles. The results are presented with the same four discharges for both throttles and both methods. The given discharge is through the turbine, and the water flow through the throttle will not be the same. All loss coefficients are related to the water flow in the pipe over under the throttle. The results are first presented for the physical model, then the numerical model and at last the three methods are presented in the same figures for comparison. The two throttle designs are presented individually. Finally some additional findings are presented.

### 5.1 First throttle design

The first throttle design was made with a smallest diameter of 25 mm and the protruding pipe was 2 mm thick and approximately 0.6 mm thick at the edge. Literature values gave loss a coefficient of 257 for upward flow and 389 for downward flow, which give a ratio of 1.51 between the loss coefficients in upward and downward direction.

#### 5.1.1 Physical model

Figure 5-1 shows the results from the physical model tests for the 25 mm throttle for upward flow, and figure 5-2 for downward flow. The loss coefficients are presented in a stock chart, which shows the minimum, maximum and the average values for the four investigated discharges. The reason for variation is discussed in the discussion chapter.

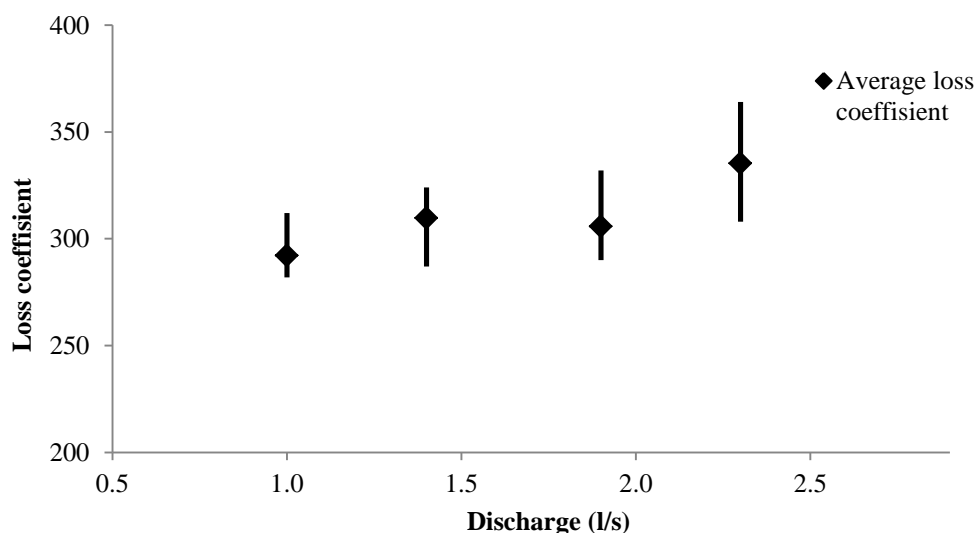


Figure 5-1: Stock chart of the loss coefficients with upward flow for the 25 mm throttle.

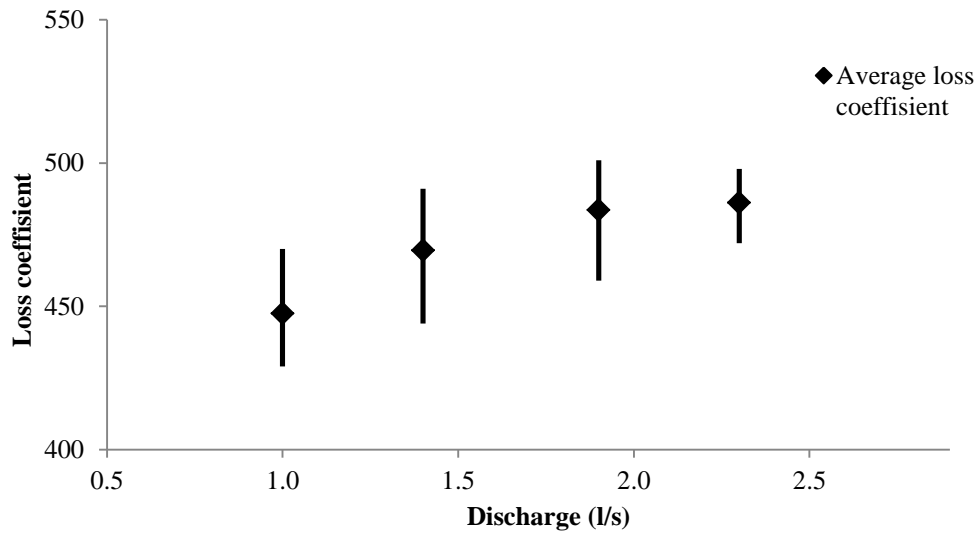


Figure 5-2: Stock chart of the loss coefficients with downward flow for the 25 mm throttle.

Table 5-1 shows the average loss coefficients and the loss ratios for the physical experiments with the 25 mm throttle.

Table 5-1: Loss coefficients and loss ratios from the physical experiments with the 25 mm throttle.

Discharge (l/s)	Upward	Downward	Ratio
1.0	290	447	1.54
1.4	307	468	1.52
1.9	303	482	1.59
2.3	331	485	1.46

### 5.1.2 Numerical model

Table 5-2 shows the results from the 3D numerical model simulations with the 25 mm throttle.

Table 5-2: Loss coefficients and loss ratios from the 3D numerical simulations of the 25 mm throttle.

Discharge (l/s)	Upward	Downward	Ratio
1.0	259	570	2.19
1.4	259	572	2.20
1.9	259	573	2.21
2.3	259	575	2.22

5.1.3 Comparison

Figure 5-3 shows the loss coefficients for the three different methods with the 25 mm throttle for upward flow, and figure 5-4 for downward flow.

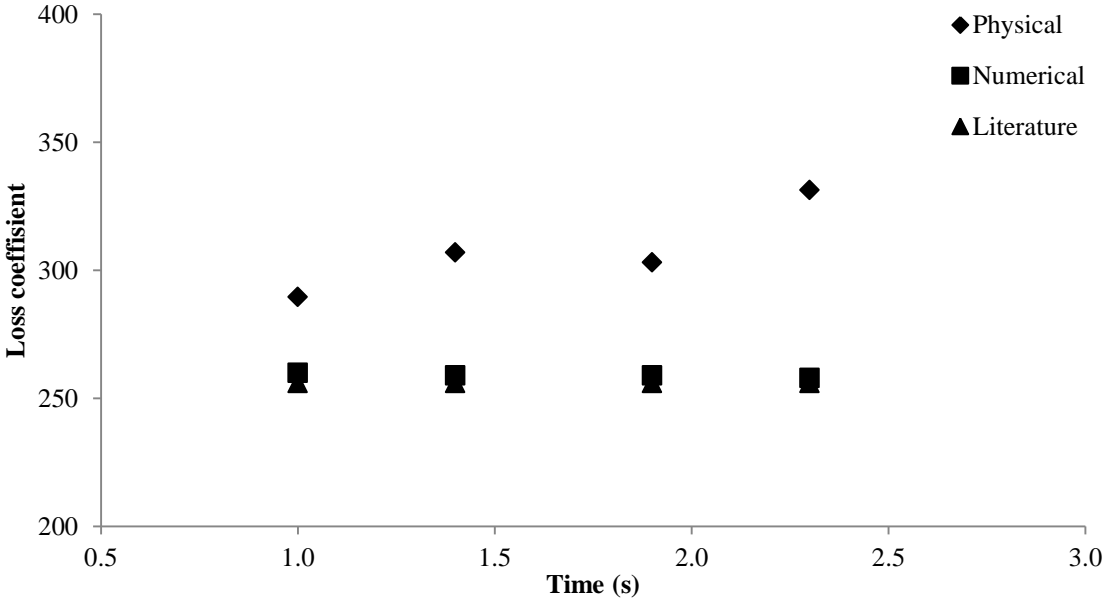


Figure 5-3: Loss coefficients 25 mm throttle upward flow.

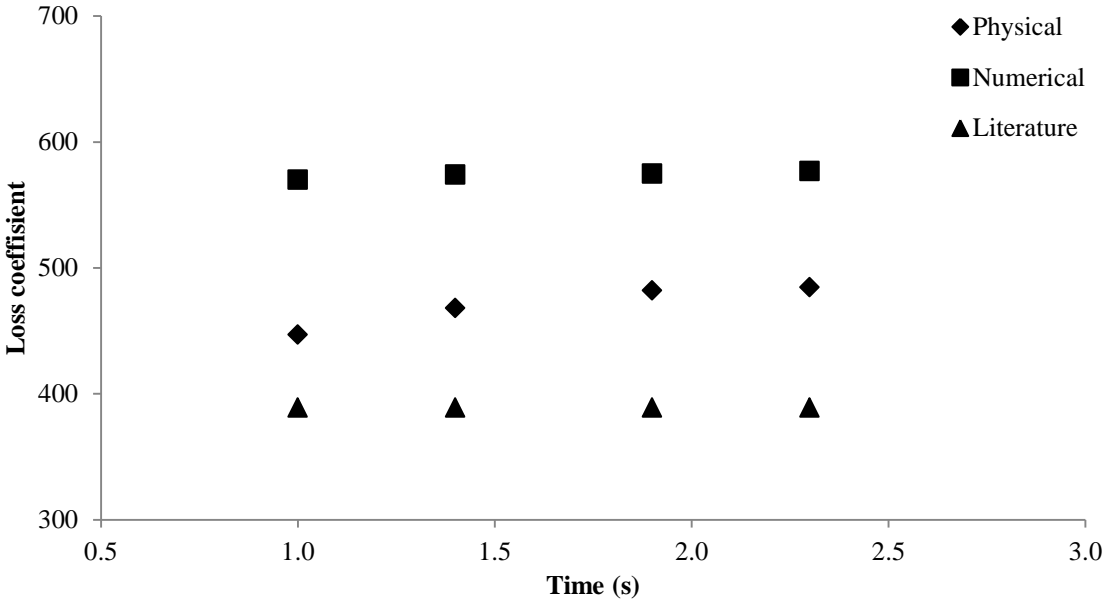


Figure 5-4: Loss coefficients 25 mm throttle downward flow.

## 5.2 Second throttle design

The second throttle design was made with a smallest diameter of 23 mm, and the protruding pipe was 1 m thick and approximately 0.2 mm at the edge. Literature values gave loss a coefficient of 364 for upward flow and 620 for downward flow, which give a ratio of 1.70 between the loss coefficients in upward and downward direction.

### 5.2.1 Physical model

Figure 5-5 shows the results from the physical model tests for the 23 mm throttle for upward flow, and figure 5-6 for downward flow. The loss coefficients are presented in a stock chart, which shows the range for the minimum, maximum and the average values for the four investigated discharges.

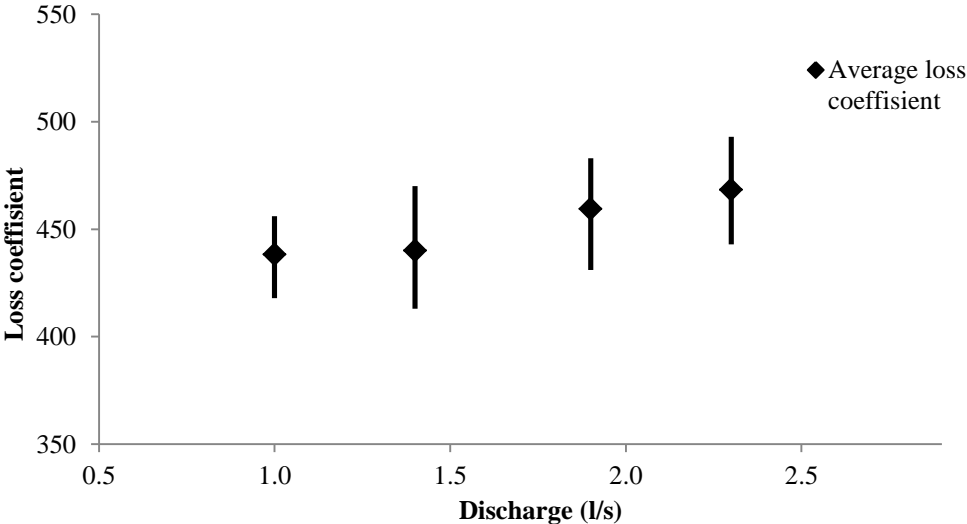


Figure 5-5: Stock chart of the loss coefficients with upward flow for the 23 mm throttle.

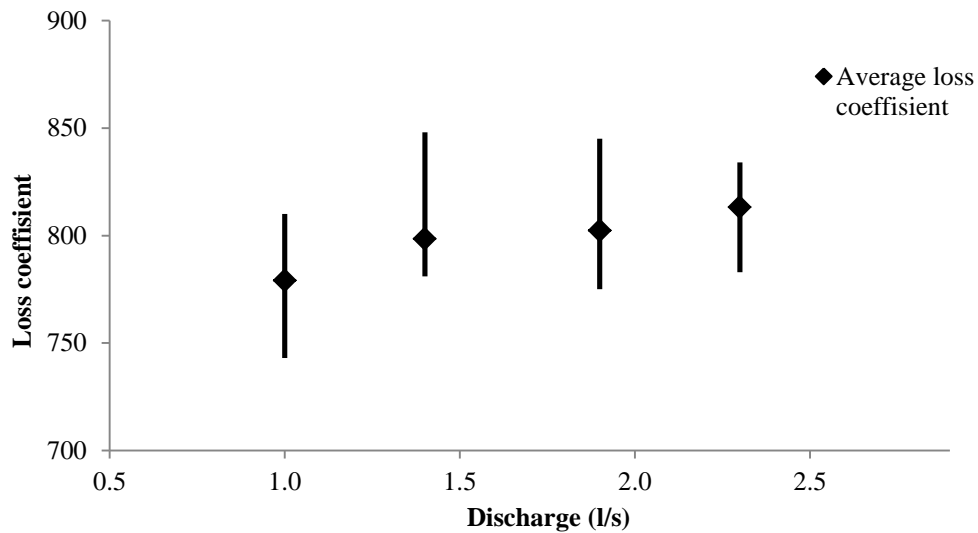


Figure 5-6: Stock chart of the loss coefficients with downward flow for the 23 mm throttle.

Table 5-3 shows the average loss coefficients and the loss ratios for the physical experiments with the 23 mm throttle.

Table 5-3: Loss coefficients and loss ratios from the physical experiments for the 23 mm throttle.

Discharge (l/s)	Upward	Downward	Ratio
1.0	436	778	1.79
1.4	437	797	1.82
1.9	456	800	1.75
2.3	464	812	1.75

### 5.2.2 Numerical model

Table 5-4 shows the results from the 3D numerical model simulations of the 23 mm throttle.

Table 5-4: Loss coefficients and loss ratios from the 3D numerical simulations of the 23 mm throttle.

Discharge (l/s)	Upward	Downward	Ratio
1.0	379	856	1.98
1.4	379	860	1.98
1.9	378	863	1.99
2.3	378	864	1.99

### 5.2.3 Comparison

Figure 5-7 shows the loss coefficients for the 23 mm throttle with upward flow for the three different methods, and figure 5-8 shows the loss coefficients for downward flow.

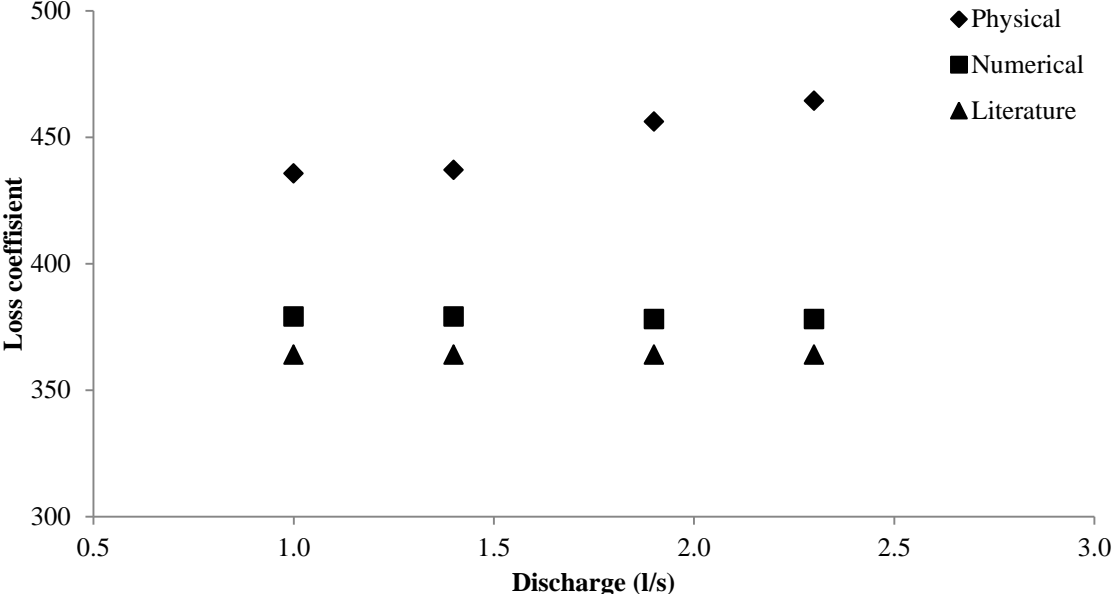


Figure 5-7: Loss coefficients 23 mm throttle upward flow.

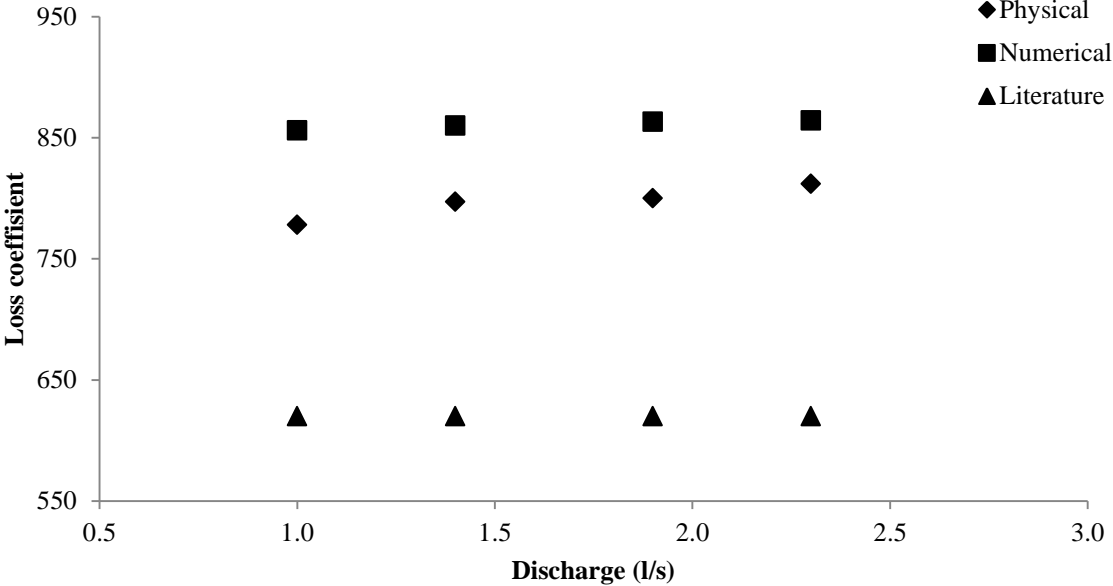


Figure 5-8: Loss coefficients 23 mm throttle downward flow.

### 5.3 Additional findings

In addition to the results from the loss coefficients the air pressure and turbine pressure from the physical model experiments are presented. Also the results from experiments with no

throttle are presented. All results are presented for the four investigated discharges and with the worst multiple opening and closing load case.

**5.3.1 First throttle design**

Figure 5-9 shows the air pressure in the air cushion surge chamber with the 25 mm throttle. The pressure in front of the turbine with the 25 mm throttle is presented in figure 5-10.

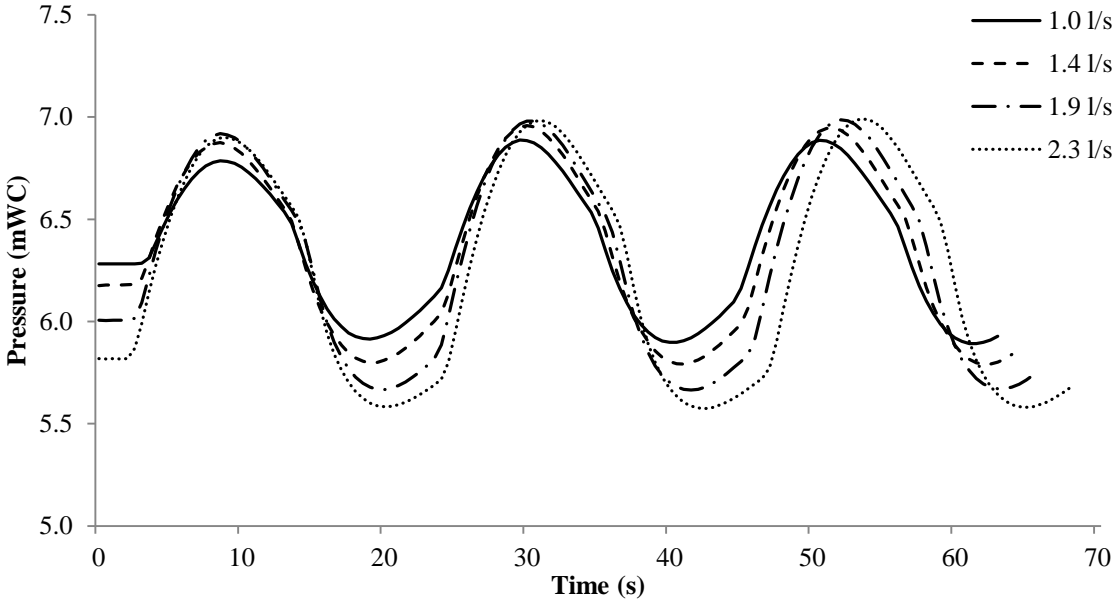


Figure 5-9: Air cushion surge chamber air pressure with the 25 mm throttle.

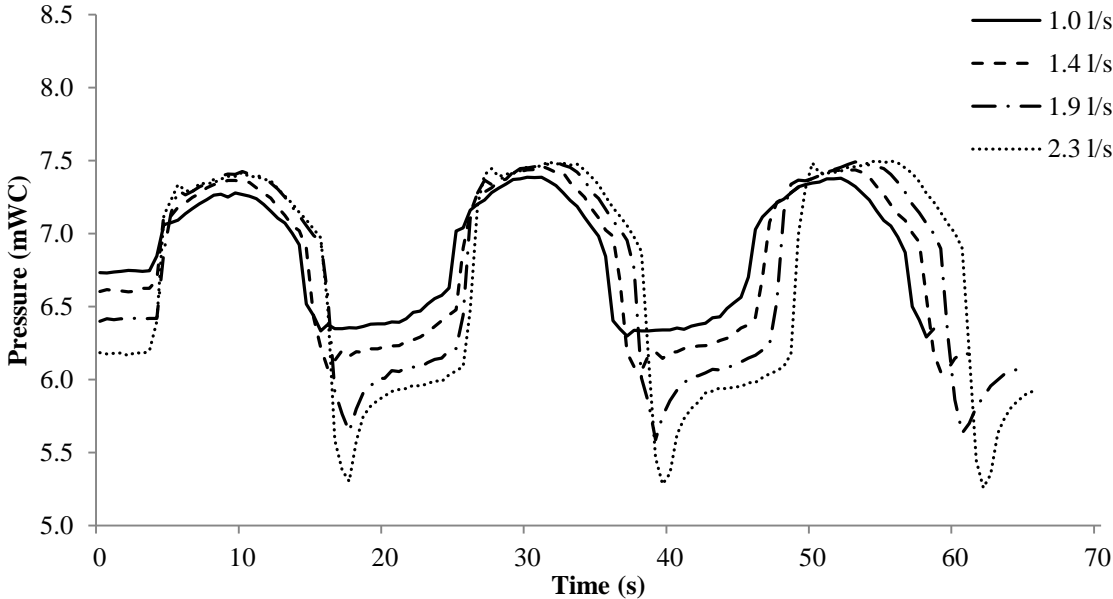


Figure 5-10: Turbine pressure with the 25 mm throttle.

### 5.3.2 Second throttle design

Figure 5-11 shows the air pressure in the air cushion surge chamber with the 23 mm throttle. The pressure in front of the turbine with the 23 mm throttle is presented in figure 5-12.

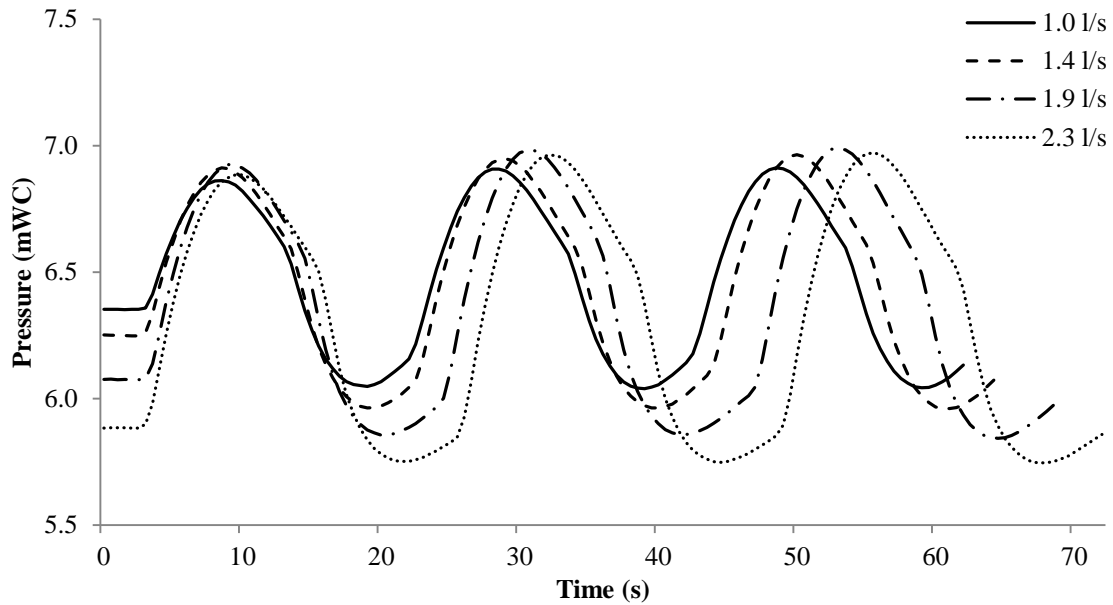


Figure 5-11: Air cushion surge chamber air pressure with the 23 mm throttle.

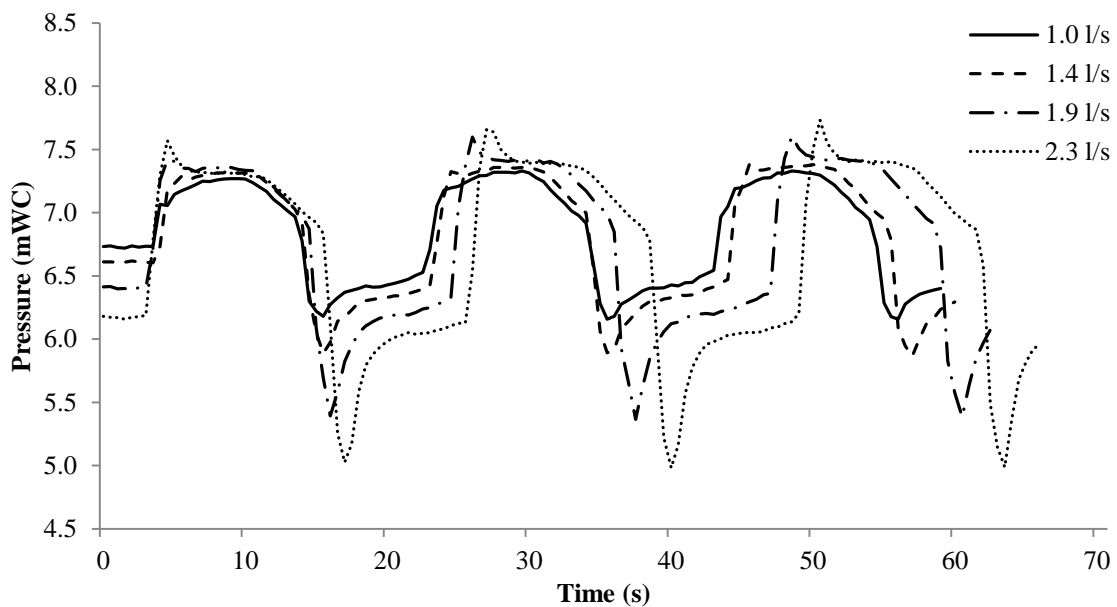


Figure 5-12: Turbine pressure with the 23 mm throttle.



5.3.3 No throttle

Figure 5-13 shows the air pressure in the air cushion surge chamber with no throttle installed. The pressure in front of the turbine with no throttling is presented in figure 5-14.

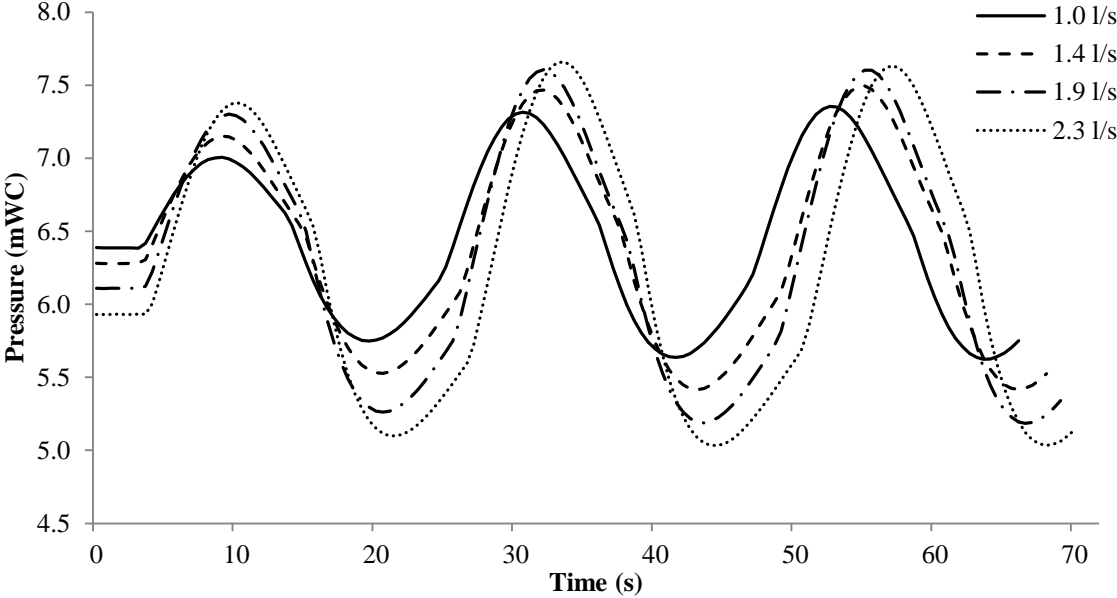


Figure 5-13: Air cushion surge chamber air pressure with no throttle.

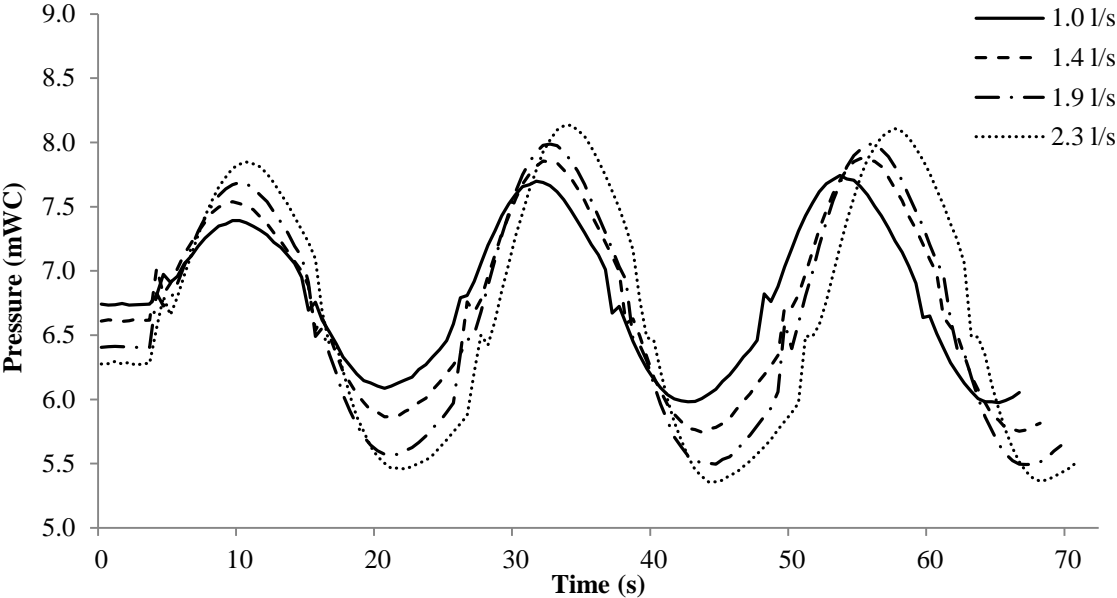


Figure 5-14: Turbine pressure with no throttle.



## 6 Discussion

This chapter discusses the results from the experiments. First the results for the throttle effects are discussed, and then possible error sources are discussed and at last the additional findings. The additional findings discuss the effect the introduction of a surge tank throttle has on the physical model.

### 6.1 Throttle effects

Table 6-1 shows the maximum and minimum differences between the physical and numerical model for the two throttles in both directions.

*Table 6-1: Physical vs numerical loss coefficients.*

Physical vs numerical			
Throttle	Direction	Difference	Higher/lower
23 mm	Upward	56-86	Higher
23 mm	Downward	52-78	Lower
25 mm	Upward	30-75	Higher
25 mm	Downward	90-123	Lower

Table 6-2 shows maximum and minimum difference between the physical model and the literature values for the two throttles in both directions.

*Table 6-2: Physical vs literature loss coefficients.*

Physical vs literature			
Throttle	Direction	Difference	Higher/lower
23 mm	Upward	72-100	Higher
23 mm	Downward	159-193	Higher
25 mm	Upward	34-75	Higher
25 mm	Downward	63-101	Higher

Table 6-3 shows the maximum and minimum difference between literature loss coefficients and the numerical loss coefficients for the two throttles in both directions.

Table 6-3: Literature vs numerical loss coefficients.

Literature vs numerical			
Throttle	Direction	Difference	Higher/lower
23 mm	Upward	14-15	Lower
23 mm	Downward	237-245	Lower
25 mm	Upward	2-4	Lower
25 mm	Downward	186-193	Lower

Similarities for both throttles in both directions are that the literature values are the lowest, and underestimate the head loss coefficient compared to the physical model tests. The physical model value also has a tendency to increase with increasing discharge for all situations. This increase may be due to the increased water flow which may cause a stronger contraction through the throttle, and therefore also a higher loss. In addition, the model had a tendency to drag some air that was accumulated and pushed through the throttle in some cases of upward flow when the discharge was increased (although the model was run for a long time). This may also cause increased loss in upward direction with increased discharge. The deviations between the different methods are smallest for the largest throttle, and highest for the smallest throttle for all cases except between the physical and numerical in downward flow. For this case the 25 mm throttle has the largest deviation. The numerical and literature loss coefficients are both relative stable for all discharges, with a small increase for the numerical simulations.

The 3D numerical simulations give slightly higher loss coefficients than the literature for upward flow, and significantly higher for downward flow. This agrees with the findings in Gabl et al. (2011), where numerical simulations of a throttle were compared with different literature sources, and the literature values were found to be slightly lower for upward flow and much lower for downward flow.

The results for upward flow are quite similar for both throttles, where the numerical and literature values are almost the same, and show acceptable correlation to the physical model test. The physical values are higher for both throttles. For downward flow the numerical values are highest for both throttles. The numerical and physical are quite similar for downward flow for the 23 mm throttle, but for the 25 mm throttle the difference is larger. The hydraulic conditions in the downward direction are more complicated, and this is also reflected in the results.

The 25 mm throttle has an average ratio of 1.53 for the physical model, 2.2 for the numerical and 1.51 for literature values. While the 23 mm throttle has an average ratio of 1.78 for the physical model, 1.9 for the numerical and 1.70 for literature values. The reason for the lower ratio for the 25 mm throttle in the physical experiments is the thickness and shape of the protruding pipe element. This was made 1 mm tick for the 23 mm throttle and 2 mm tick for the 25 mm throttle, and also the edge of the protruding pipe was sharper for the 23 mm throttle. The thinner and sharper pipe element results in a higher loss in downward direction for the 23 mm throttle, and therefore also a higher ratio. The numerical simulations showed that this had no effect with upward flow, as the literature review stated. The ratio between the

upward and downward loss coefficients are pretty equal for the physical and the literature values, while the numerical simulations gives a much higher ratio, especially for the 25 mm throttle. This high ratio is a result of the upward loss coefficient is lower than the physical value and the downward is higher.

As the stock diagrams in the result chapter shows, there is a quite large spread in the results from the physical model, for flow in both directions, but the largest spread seems to be with downward flow. This is the reason for doing several experiments with each throttle and for each discharge and only use the best results to find the average values.

## 6.2 Error sources

The physical model used in this thesis is not optimal for only finding the head loss in a throttle due to the large construction and the fact that it is built to investigate the whole system and not only the throttle. For this purpose a simpler model would be better, and the numbers of error sources could then be reduced. For example a horizontal model where there is a straight pipe in both side of a throttle, and a possibility for controlling the exact water flow through the model would be better to find the throttle loss. In both sides of the throttle pressure gauges must be mounted. The layout would give the loss caused by the throttle with more accuracy, and the water flow would not be any error source like in model used in this thesis. But in this kind of layout the water flow must be found from a numerical model and then used in the physical. This kind of hybrid modelling is often used in Austria when the surge tanks are investigated. They often build just the surge tank construction and use numerical models to calculate the inflow and outflow. The physical model used in this thesis is on the other hand good to investigate the effect a throttle have on the whole hydraulic system, like the pressure in the air cushion and in front of the turbine. In addition, the dampening effect can be tested, and there is no need to use a numerical model to find the water flow through the throttle.

The pressure gauges were last calibrated a year ago, and may therefore not be correct calibrated at the time the experiments were conducted. This could introduce a small error in the results.

The water flows used to calculate the velocity in the loss coefficients calculations is not measured directly from the physical model, but they are calculated with respect to the pressure change in the air cushion surge chamber with equation (3.2) from the theory. An adiabatic constant of 1.4 is also assumed. Errors in the water flows would directly affect the local loss coefficients found from the physical experiments, and this is one of the most important error sources. In further work this should be attempted to be reduced, but it is difficult without making a new model.

The timing of the opening and closing is also important for the results, and this will also affect the water flow. For both throttles and each investigated discharge several experiments were conducted. After an experiment where conducted the water flow was calculated and the

timing was inspected. Only the experiments with good timing were used in further calculations. In the numerical simulations it was much easier to get correct timing due to the possibility of monitoring the flow in the connection pipe and the possibility of pause the simulations. Experiments showed that a little different in the opening and closing did not affect the pressure rise and lowering so much, as long as the timing was not too late. In this case the water had turned around and it must then change flow direction again. Too late timing will have large influence on the maximum and minimum water flow, and the pressure development. Figure 6-1 shows the flow in and out from the air cushion surge chamber calculated from the pressure in the physical model with a discharge of 1.4 l/s and the 23 mm throttle for two different experiments.

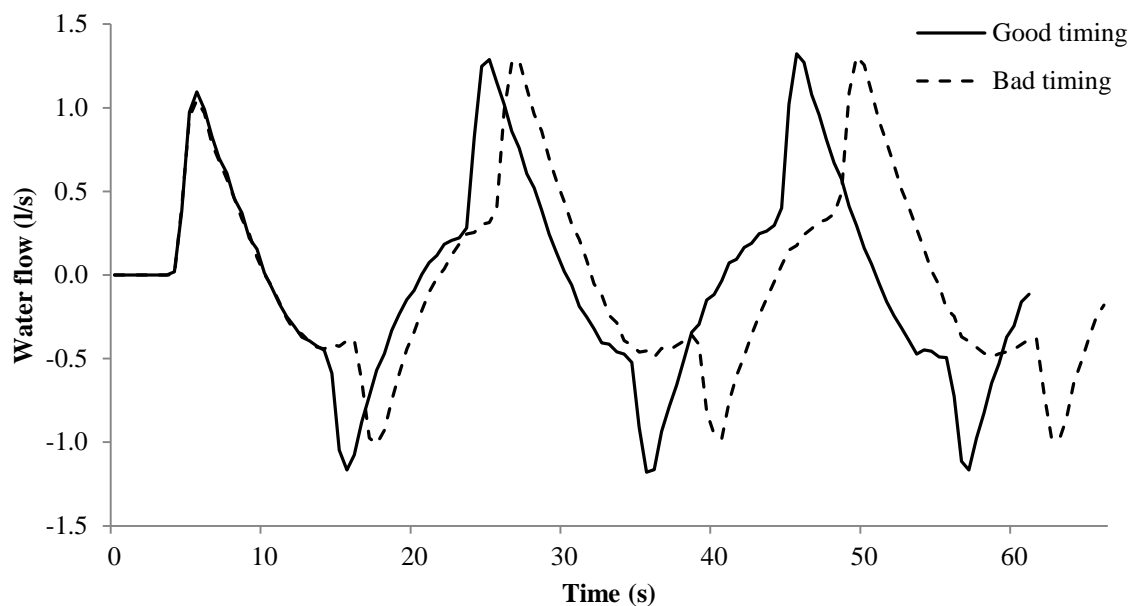


Figure 6-1: Water flow in and out from air cushion surge chamber with 1.4 l/s discharge.

The figure shows an experiment with good timing and one with bad timing for the opening of the turbine. This clearly shows the effect on the downward flow, but the upward is almost the same. The bad timing experiment in the figure was not used in any further calculation, but it shows how small differences in the timing quickly affect the water flow and then also the loss coefficients.

The experiments were conducted with a sample frequency of 1000 Hz, and the log was set to 500 samples per mean, which was a compromise between accuracy and noise in the measurements. As can be seen in figure 6-1, some of the peaks are nice and sharp, but in some cases they are more flat. The pressure on the other hand would be about the same in both cases, and how the water peaks are therefore affecting the loss coefficients. When the peak is flat and the pressure different are the same, this would give too little water flow and a higher loss coefficient as the head loss is divided by a smaller number. If the log was set coarser, for example 1000 samples per mean this would be too rough and give many flat peaks. But if the log was set finer, for example 100 samples per mean this would give too much noise in the

results, and calculation would be different. Therefore, 500 samples per mean were chosen as a compromise between accuracy and noise.

The friction is neglected in the calculations of the loss coefficients for all methods, and this could be an error source in the physical model since it is not considered but it is still there. This simplification is believed to have a very little effect due to the short distance between the pressure gauges and due to the smooth surface in the steel pipes. But this may cause the loss coefficients from the physical values to be a little too high since this small friction loss is included.

In case of downward flow the velocity height at the lowest pressure gauge is neglected. This is assumed to have little impact on the results due to very small values as a result of low water velocity in the physical model. In the case of upward flow the pressure shaft is in theory plugged, and the velocity is zero, and therefore no velocity height. The other pressure gauge is placed in the air cushion, and there is therefore no velocity height here either.

The center of the T-connection in the physical model is placed 12 cm under the bottom of the throttle, and this was believed to have influence on the results from the experiments. The additional loss was believed to come as a result of the jet flowing right into the pipe wall and also some loss due to the change in stream direction. Some numerical simulations with 2.3 l/s water flow were conducted to investigate the effect of the T-connection. 2.3 l/s were chosen because this would give the highest water velocity in the throttle, and therefore also the strongest jet into the pipe wall under the throttle. Figure 6-2 shows a scalar scene from a numerical simulation in STAR-CCM+ with 2.3 l/s and the 23 mm throttle. Water is also flowing in from the headrace to the right, which is the situation with downsurge flow in the multiple switching case.

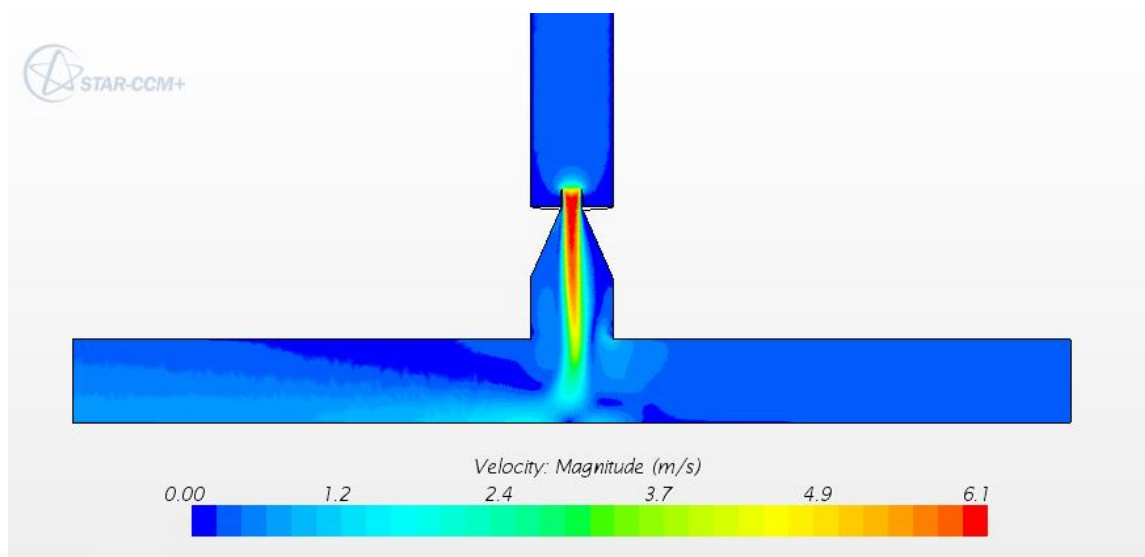


Figure 6-2: Scalar scene for downward flow with T-connection.

The numerical simulations gave a very small increase in the loss coefficient when the T-connection was included for downward flow in the simulations. This indicates that the loss coefficients in the downward direction found from the physical model may be a little larger than what is caused just by the throttle. The influence of the T-connection was also investigated for the upward flow direction with numerical simulations, and the results gave that it had no effect on the loss coefficients.

The 25 mm throttle was modified due to damage during the first tests. This was a crack in the upper flange most probably caused by too hard tightening of the bolts. The lower flange was also repaired after a leakage in the transition to the cone part. During the repair a plexiglass ring was added on the top of the upper flange for support. The ring had a diameter that was just below 0.1 m, and could affect the results. This effect is assumed to be limited due to the very small decrease in the diameter. The ring was also much lower than the length of the protruding pipe, so in case of downward flow it most probably in the dead storage and will not affect the results.

The European Research Community on Flow, Turbulence and Combustion have published Best Practice Guidelines for CFD, where they have classified the errors in CFD in seven categories (Olsen, 2012):

1. Modeling errors when modeling the real world with mathematical equations.
2. Errors in the numerical approximations due to discretization of the equations.
3. Errors due to not complete convergence.
4. Round of errors.
5. Errors in boundary conditions.
6. Human errors due to inexperience of the user.
7. Bugs in the software.

The possible error sources in the 3D numerical simulations done in this thesis are most likely due to human errors due to inexperience of the user. There are a lot of choices to be made, and there is easy to make errors or some choices that not are optimal. However the residuals, the scalar and the vector plots were satisfactory without any indication of errors. Among the other categories, errors in the boundary conditions may be a possible source of error. The velocity is found from the 1D numerical simulations and it may therefore not be correct in comparison with the physical model. But as the results show the loss coefficient in the numerical simulations are pretty constant depending on the discharge, so this is believed to have little impact. The pressure is also set to the same in both directions. This was confirmed to not have any effect on the loss calculations by doing a test with changed pressure in the downward direction. After all the geometry is pretty simple, and there is not so many uncertainties in the boundaries, so the calculations is most probably correct. The other types of error sources listed are believed to have little impact on the simulations.

In the literature values there may be some uncertainties in the formulas and tables found and presented, but this will not be discussed in more details. In the choices made in the calculation there are most uncertainties connected to the selected value of  $m$ . This was set to 10, which corresponds to an almost rectangular velocity profile. The  $m$  value has the largest impact



when it is small, and already from around 8 it has very little impact on the results and the solution would be almost constant. But when it is smaller it will quickly affect the results much. Small  $m$  values correspond to more rectangular velocity profiles, which is typical for laminar flow conditions. If a too small value of  $m$  is chosen this will give a too high expansion loss, and a too high value will give a too low expansion loss. The flow in the physical model is clearly turbulent, and the chosen  $m$  value should not affect the results much.

Another uncertainty in the literature value is the thickness of the edge of the protruding pipe. This is important for the sudden contraction loss for downward flow, and a small change in this will quickly affect the results. The thickness of the protruding pipe and the edge of it was measured with a digital caliper, but the edge is still hard to get precisely. A thinner and sharper protruding pipe will give a higher loss ratio, and a thicker edge will give a lower loss ratio. The other values and coefficients are calculated or found when the rest of the throttle parameters are decided, and there are no large uncertainties in these.

### 6.3 Additional findings

In addition to the throttle head loss, the effect the throttle has on the whole system will be discussed. In the discussion of the throttle effect the results from the experiments with the 23 mm throttle is used. This is because this was closest to the optimal for the scaled maximum discharge from the prototype, and therefore also had the highest impact with this discharge. Figure 6-3 and shows the pressure development in front of the turbine in the physical model with no throttle and with the 23 mm throttle. The discharge through the turbine (valve) is 1.4 l/s, and this gave an almost perfect pressure for this throttle with a multiple switching situation.

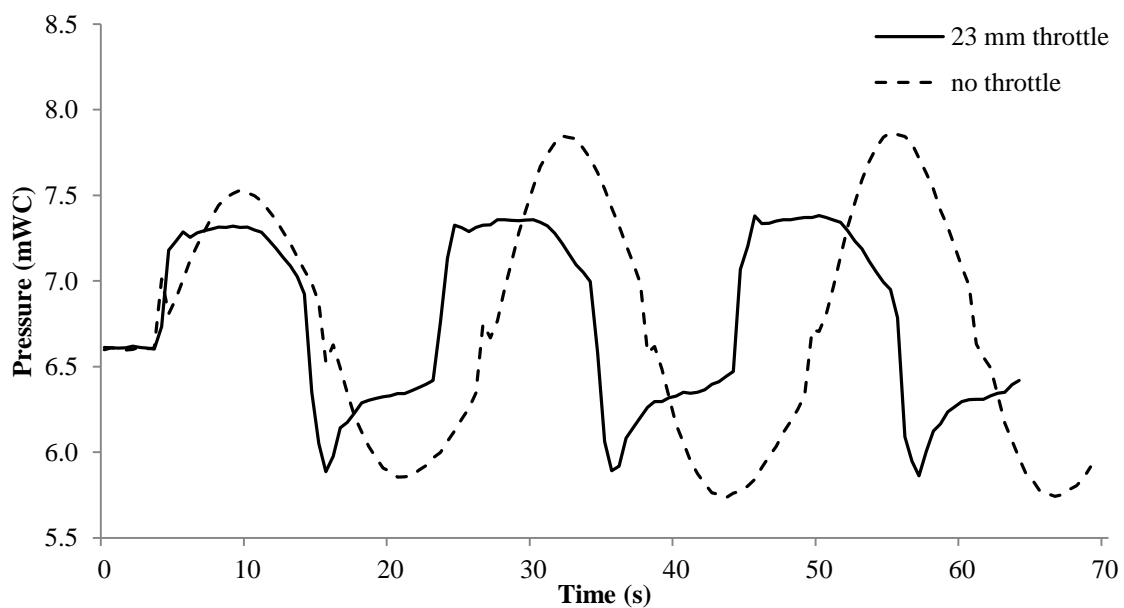


Figure 6-3: Pressure in front of turbine with and without a throttle with 1.4 l/s through the turbine.

The figure shows a significant effect by introducing the throttle, where the highest pressure in front of the turbine (valve) is 0.5 mWC lower for the throttled experiment. Figure 6-4 shows the pressure in front of the turbine with the 23 mm throttle and 1.0 l/s, which is the scaled maximum discharge from the prototype.

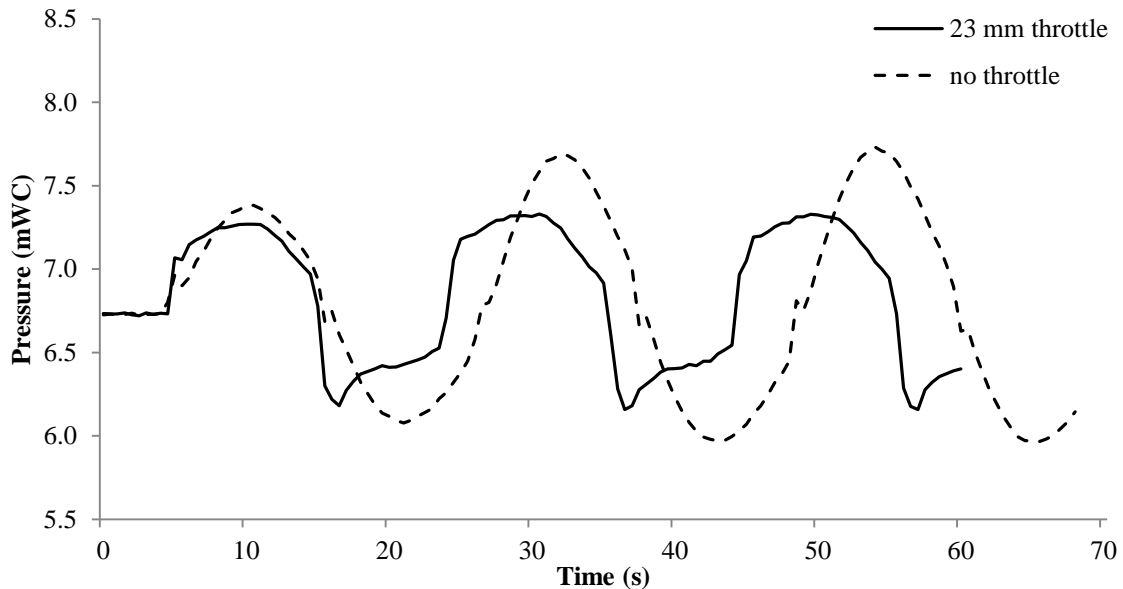


Figure 6-4: Pressure in front of turbine with and without a throttle with 1.0 l/s through the turbine.

The pressure in front of the turbine is 0.4 mWC lower at the maximum and 0.2 mWC higher for the minimum. The model is a 1:65 scale model of the prototype, which means that the maximum pressure decreasing corresponds to 26 mWC in the prototype. The 23 mm throttle was close to optimal for a discharge of 1.4 l/s, which means that for 1.0 l/s it could probably have a little bit smaller diameter, and the pressure decreasing could be even higher.

Figure 6-5 shows the pressure development in the air cushion surge chamber for a multiple switching situations with and without the 23 mm throttle in the system with a discharge of 1.0 l/s.

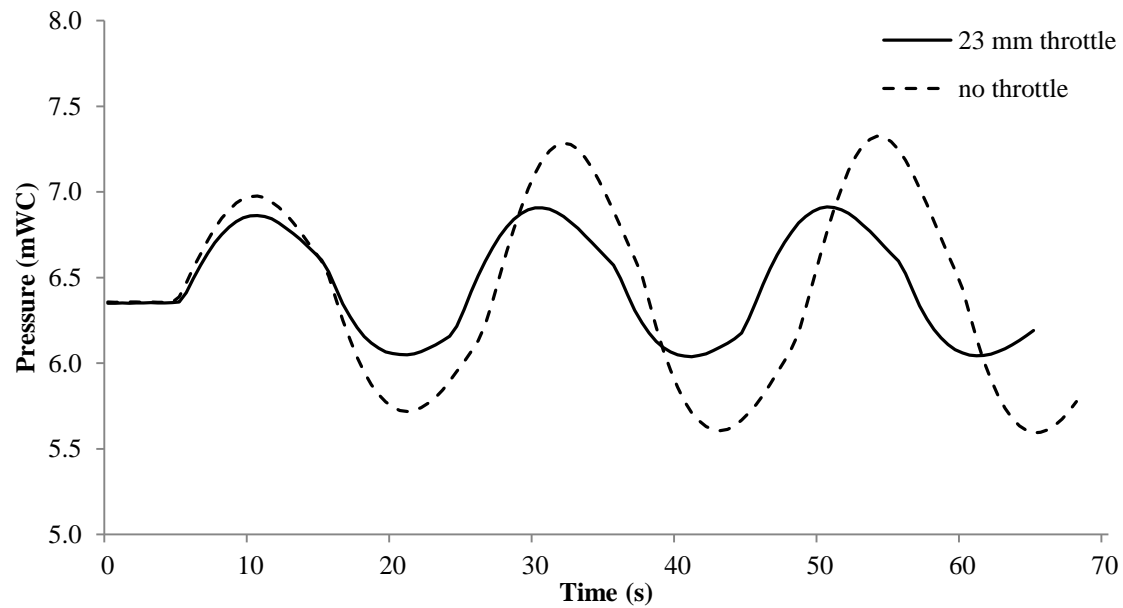


Figure 6-5: Pressure in air cushion surge chamber with 1.0 l/s discharge.

Also for the surge chamber the throttle has a significant impact on the pressure, where the maximum air pressure is 0.4 mWC lower with the throttle, and 0.4 mWC higher at the minimum. This corresponds to 26 mWC in the prototype. For a power plant with a simple surge shaft the maximum and minimum upsurge and downsurge in meters corresponds to the pressure in the air cushion for an equivalent cross section. Formulas for the equivalent cross section can be found in literature, for example in Nielsen (1990). This means that a similar power plant layout with a traditionally Norwegian surge shaft instead of an air cushion surge chamber can move the upsurge and downsurge limits with 26 meters if the surge shaft has an equivalent cross section to the air cushion surge chamber in the prototype. If the cross section is larger this upsurge and downsurge limits will be lower. This can be beneficial if the project is on the limits of the topography, and it gives better security against getting free water surface in the headrace tunnel. For an existing power plant with such problems, it is clearly an option to install a throttle.

Figure 6-6 shows the water level development in the air cushion surge chamber with and without a throttle. The water level is shown in cm above or below the water level during steady operation with 1.0 l/s through the turbine.

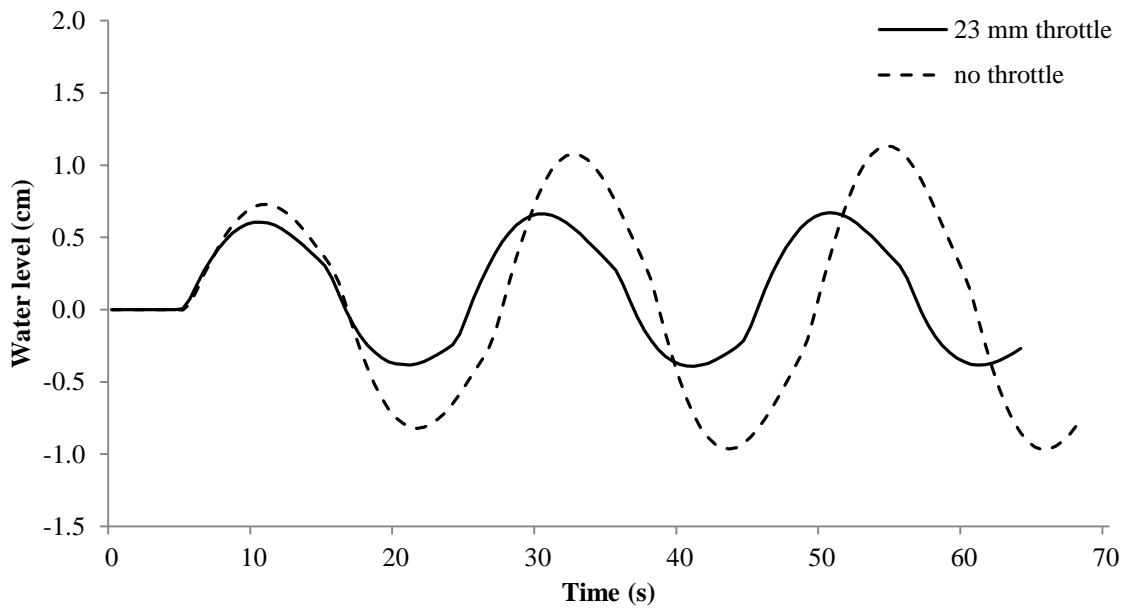


Figure 6-6: Water level in air cushion surge chamber.

The water level is calculated from the pressure change in the air cushion, and the development is therefore the same. The surge tank throttle gives a maximum water level 0.5 cm lower and 0.6 cm higher for the maximum downsurge. This corresponds to 2.6 and 3.9 meters in the prototype. Figure 6-7 shows the pressure development in the air cushion surge chamber after a single shut down in the physical model with the 23 mm throttle and with no throttling.

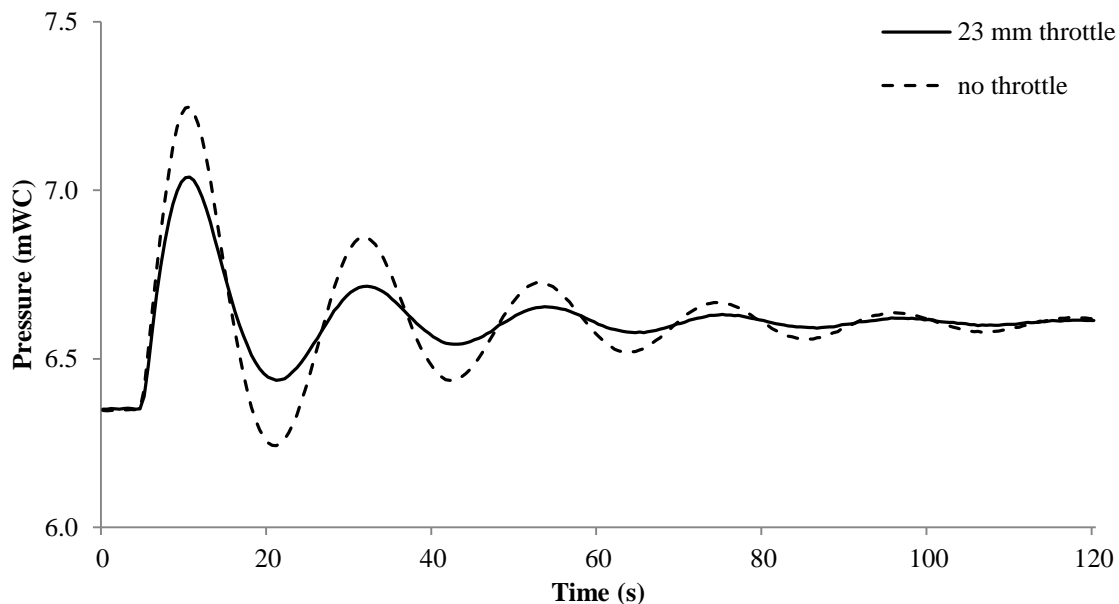


Figure 6-7: Dampening effect with and without a throttled in the physical model.

This shows that the throttle has a significant impact in the dampening of the mass oscillations in the system. After about 100 second the throttled system is almost dampen out, but with no throttle there is still some oscillations. The figure shows the pressure development with a discharge of 1.4 l/s, which was the optimal discharge for the 23 mm throttle with a multiple

switching situation. For a single shut down situation the throttle diameter could be even smaller, as seen in the first peak in figure 6-3.

The figures show that the throttle has a significant impact on the pressure development and dampening of the whole system. This agrees with the findings in the literature review, where the throttle was seen to have impact on the pressure in the air cushion and in front of the turbine, better dampening effect on the mass oscillations and lowering of the surge tank volume. For later research it could be of interest to see how good the results would be if the optimal throttle found in the physical model is scaled up and put into a full scaled power plant, in order to find out if it is possible to design a throttle in a model. As a starting point this could be done with a 1D numerical model, but it would also be interesting to do research on an existing power plant if installation of a surge tank throttle is considered.



## 7 Conclusion

The three methods give quite similar results with simple hydraulic conditions, but when the hydraulic conditions become more complicated they differ more.

The literature values underestimate the head loss coefficient in both directions compared to the physical model test. In upward direction the literature values show acceptable correlation to the physical model test, which is the direction with the simplest hydraulic conditions. The conditions in the downward direction are more complicated, and this is also reflected in the results, where the difference is larger, especially for the smallest throttle.

The 3D numerical simulations give results that are lower than the physical model test for downward flow, and higher for upward flow. The numerical simulations give the highest ratio between head loss in the upward and downward directions

The findings also show a significant impact on the pressure development and dampening of mass oscillations by inserting a surge tank throttle, as was found in the literature review. The two throttles tested in the physical model reduced the maximum pressure by 5.2% and 3.9% for the smallest and largest throttle diameter respectively. This was with the use of the scaled maximum discharge from the prototype.

### 7.1 Suggestions for further work

The physical model used in this thesis is not optimal for only finding the head loss in a throttle. In further work it is recommended to build a simpler model to decide the throttle head loss and be able to reduce the number of error sources. This may for example be a horizontal model where there is a straight pipe in both sides of a throttle, and a possibility for controlling the exact water flow through the model. In both sides of the throttle pressure gauges must be mounted. This layout would probably give the head loss caused by the throttle with more accuracy. Such a layout could however not be used to investigate how the throttle affects the pressure development in a power plant system, and the optimal throttle loss and discharges must be found with numerical simulations.

It will also be of interest to test how the optimal throttle found from the physical model works in a full size power plant, in order to find out if there is possible to design a throttle with the help of a physical model. As a start this could be done by upscale the throttle and see how it works in a full size 1D numerical model, but if an existing power plant considering to install a throttle this would be very useful to do research on.





---

## References

- CD-ADAPCO. 2015. *STAR-CCM+ user guide* [Online].
- CROWE, C. T., ELGER, D. F., WILLIAMS, B. C. & ROBERSON, J. A. 2009. *Engineering fluid mechanics*, Hoboken, N.J., Wiley.
- GABL, R., ACHLEITNER, S., NEUNER, J. & AUFLEGER, M. 2014. Accuracy analysis of a physical scale model using the example of an asymmetric orifice. *Flow Measurement and Instrumentation* 36 (2014).
- GABL, R., ACHLEITNER, S., NEUNER, J., GÖTSCH, H. & AUFLEGER, M. 3D-numerical optimisation of an asymmetric orifice in the surge tank of a high-head power plant. 34th IAHR World Congress-Balance and uncertainty, 2011 26 June - 1 July 2011, Brisbane, Australia.
- GOODALL, D. C., BROCH, E., TEKLE, T. & KJØRHOLT, H. 1988. Air cushion surge chambers for underground power plants. *International Water Power & Dam Construction*.
- GUTTORMSEN, O. 2006. *Vassdragsteknikk II*, Trondheim, Tapir, Kompendieforlaget.
- HU, J., SOU, L., ZHANG, J. & FANG, J. 2007. Advance in research on air cushion surge chamber in hydropower plant. *ASME International Mechanical Engineering Congress and Exposition*. November 11-15, 2007, Seattle, Washington, USA.
- IDELCHIK, I. E. 1986. *Handbook of hydraulic resistance*, Washington, Hemisphere Publ.
- MOODY, L. F. & PRINCETON, N. J. 1944. Friction Factors for Pipe Flow. *Transactions of the A.S.M.E.*
- NIELSEN, T. K. 1990. Dynamisk dimensjonering av vannkraftverk. Trondheim: SINTEF.
- OLSEN, N. R. B. 2012. *Numerical Modelling and Hydraulics, 3rd edition*
- RICHTER, W., DOBLER, W. & KNOBLAUCH, H. 2012a. Hydraulic and numerical modelling of an asymmetric orifice within a surge tank. *4th IAHR International Symposium on Hydraulic Structures*. Porto, Portugal.
- RICHTER, W., KNOBLAUCH, H. & LARCHER, M. 2012b. Transient Model Test of Surge Tank Reisseck 2. *IAHR Congress*.

- RICHTER, W., ZENZ, G., SCHNEIDER, J. & KNOBLAUCH, H. 2015. Surge tanks for high head hydropower plants-Hydraulic layout-New developments. *Geomechanics and Tunnelling* 8(2015), No 1.
- STEYRER, P. 1999. Economic surge tank design by sophisticated hydraulic throttling. *International Association for Hydraulic Research Biennial congress; 28th, International Association for Hydraulic Research.*
- SVINGEN, B. 2007. Manual LVTrans for versjon 8\_1.2.4. SINTEF Energiforskning AS.
- VEREIDE, K., LIA, L. & NIELSEN, T. 2014. Physical Modelling og Hydropower Waterway with Air Cushion Surge Chamber. *5th International Symposium on Hydraulic Structures*. Brisbane, Australia, 25-27 June 20014.
- VEREIDE, K., RICHTER, W., ZENZ, G. & LIA, L. 2015. Surg Tank Research in Austria and Norway. *WasserWirtschaft Extra*, 1, 58-62.
- WYLIE, E. B., STREETER, V. L. & SUO, L. 1993. *Fluid transients in systems*, Englewood Cliffs, NJ, Prentice Hall.